FINDING SIMPLICITY IN THE COMPLEX SYSTEMIC ARTERIAL SYSTEM : BASIS OF INCREASED PULSE PRESSURE

A Dissertation

by

MOHAMMAD WAQAR MOHIUDDIN

Submitted to the Office of Graduate Studies of
Texas A&M University
in partial fulfillment of the requirements for the degree of

DOCTOR OF PHILOSOPHY

May 2008

Major Subject: Biomedical Sciences

FINDING SIMPLICITY IN THE COMPLEX SYSTEMIC ARTERIAL SYSTEM :

BASIS OF INCREASED PULSE PRESSURE

A Dissertation

by

MOHAMMAD WAQAR MOHIUDDIN

Submitted to the Office of Graduate Studies of
Texas A&M University
in partial fulfillment of the requirements for the degree of

DOCTOR OF PHILOSOPHY

Approved by:

Chair of Committee,	Christopher Quick
Committee Members,	Glen Laine
	John Stallone
	James Moore Jr.
Head of Department,	Glen Laine

May 2008

Major Subject: Biomedical Sciences

ABSTRACT

Finding Simplicity in the Complex Systemic Arterial System:

Basis of Increased Pulse Pressure.

(May 2008)

Mohammad Waqar Mohiuddin, B.Sc., Bangladesh University of Eng. & Technology;

M.S., Texas A&M University

Chair of Advisory Committee: Dr. Christopher Quick

Arterial pulse pressure is critically important to a number of diseases such as isolated systolic hypertension, coronary artery disease and heart failure. Determining the cause of increased pulse pressure has been hampered for two reasons. First, pulse pressure results from contraction of the heart and the load formed by the complex arterial tree. Pressure pulses travel from the heart to the peripheral arteries. As they reach a bifurcation or change in arterial wall properties, some of the pulses get reflected and propagate retrograde towards the heart. Second, two different modeling approaches (0-D and 1-D) describe the arterial system. The Windkessel model ascribed changes in pulse pressure to changes in total arterial compliance (C_{tot}) and total arterial resistance, whereas the transmission model ascribed them to changes in the magnitude, timing and sites of reflection. Our investigation has addressed both these limitations by finding that a complex arterial system degenerates into a simple 2-element Windkessel model when wavelength of the propagated pulse increases. This theoretical development has yielded three practical results. First, isolated systolic hypertension can be viewed as a

manifestation of a system that has degenerated into a Windkessel, and thus increased pulse pressure is due to decreased C_{tot}. Second, the well-discussed Augmentation Index does not truly describe augmentation of pulse pressure by pulse reflection. Third, the simple 2-element Windkessel can be used to characterize the interaction among heart, arterial system and axial-flow left ventricular assist device analytically. The fact that arterial systems degenerate into Windkessels explains why it becomes much easier to estimate total arterial compliance in hypertension—total arterial compliance is the dominant determinant of pulsatile pressure.

DEDICATION

To my parents

ACKNOWLEDGEMENTS

Though only my name appears on the cover of this dissertation, a great many individuals have contributed to its production. I owe my sincere gratitude to all those who have made this dissertation possible and blessed me with a wonderful graduate experience which I will cherish forever.

I have been amazingly fortunate to have Dr. Christopher Quick as my research advisor, who gave me the courage and support to make significant track change from Mechanical Engineering to Cardiovascular Physiology. His mentorship was paramount in providing the support to grow not only as a quantitative hemodynamicist but also as an open-minded thinker, and importantly, timely clues to overcome faltered steps. A decorated 'thank you' will never be enough to return his favors. So I won't try, but I would like to let him know that I am eternally indebted to him.

I would like to thank Dr. John Stallone for his insightful suggestions which helped me to correlate mathematical modeling to physiological events.

Dr. James Moore's insightful comments and constructive criticisms helped me to take my dissertation to a higher standard.

I am grateful to Dr. Glen Laine for his support, generosity, and timely advice. His mentorship, affection and humor encouraged me throughout the program. I have learned many important aspects of academia, research and grant writing, which he shared from his own experience. I feel fortunate to have him as my committee member and department head.

The portion of the dissertation concerning interaction of heart-arterial system-LVAD contains the critical contribution of two dedicated undergraduate students. I must therefore acknowledge Tam Nguyen and Ngoc-Bich Than for their hard work to produce the basis of section 5.

I would like to extend my gratitude to my friends and colleagues. They were always there to support me whenever I struggled with research. I am fortunate to have them by my side.

My parents and brother gave support and courage throughout the time and inspired me to pursue Ph.D. since I completed my high school.

Finally, I would like to mention my best friend and wife, Jasmine. She went above and beyond the call of duty. She provided me support and care with heavenly patience and tolerated my busy weekends. She shared her inputs, thoughts and suggestions. I thank her, especially, for assisting with endless formatting of the manuscripts and this dissertation.

TABLE OF CONTENTS

Page

LIST OF FIGURES

Page

Page

Page

Page

1. INTRODUCTION

Although the arterial pulse has been recognized as the most elementary sign of life, there has been growing evidence that increased pulse pressure in the systemic arterial system is directly correlated with cardiovascular diseases, such as isolated systolic hypertension (20), coronary artery disease (116), end organ failure (54), and advanced age. Increases in pulse pressure are directly related to decreases in arterial compliances due to either natural aging or patho-physiological conditions, particularly atherosclerosis (73, 131). Increased pulse pressure is an independent risk factor for cardiovascular disease, which provides challenges to developing effective therapies. With notable advancements in measurement techniques over the past 40 years (e.g., high fidelity sensors, applanation tonometry, sphygmograph, ultrasound), investigators have reported the pressure and flow pulses at the different segments of the systemic arterial tree in human subjects of different ages (43, 71). One of the most intriguing findings is that there are noticeable differences in the morphologies of the pressure pulses at different locations of the systemic tree (69, 71). Although pressure pulses dramatically change their shape and magnitude as they travel further away from the heart, they remain relatively unchanged in elderly individuals (Fig. A-1).

Numerous scientific investigations have identified the hemodynamic parameters responsible for increased pulse pressure. This section discusses the questions that arise

---

This dissertation follows the style of *American Journal of Physiology - Heart and Circulatory Physiology.*

from of the complex topology of the systemic arterial network and propagation of pressure and flow pulses through its branches.

1.1 Conventional view of pressure pulse wave reflection

As the heart contracts, pressure pulses travel from the heart and propagate through the arterial system towards the periphery. As they travel, a portion of these waves are reflected back toward the heart from multiple locations, particularly at bifurcations (69, 91) or resistance vessels (133), where the mechanical or geometrical properties of the vessels change (77). The observed pressure therefore consists of the sum of two components—a forward-traveling pressure wave and a reflected pressure wave (11). The reflected pulse wave has been of great interest to investigators because it has been shown to change dramatically with age (69) and the onset of hypertension (71). In particular, the speed at which pressure pulses travel increases with age and hypertension is ascribed primarily to decreases in arterial compliance (74, 131). This increase in pulse wave velocity is believed to explain why the peak of the reflected wave arrives earlier in the contraction cycle, when the ventricle is still ejecting (75, 81). Furthermore, the magnitude of the reflected wave also increases with age and hypertension (71). This phenomenon has been attributed to a loss of the "impedance matching" at bifurcations that normally allow pulses to be transmitted with very little reflection (47).

Taken together, observations provided evidence that the reflected wave increases systolic pressure and the mechanical load of the heart. These interpretations, however, are based on four fundamental assumptions: 1) pulse wave reflection always augments systolic pressure, 2) an increase in aortic pulse wave velocity causes a commensurate

shift in the arrival of the reflected wave, 3) the time of arrival of the reflected wave depends on the distance to the sites of major reflection, and 4) increases in the magnitude of local reflections increase the magnitude of the reflected wave reaching the heart. These assumptions, however, have yet to be tested.

To characterize and quantify the complex interaction of the forward and reflected waves with the beating heart, animal experimentation alone will not be sufficient. Complementary use of mathematical models will provide the benefit of manipulating critical parameters one at a time, which is not possible with experimental techniques.

1.2 Use of mathematical modeling to predict pulsatile hemodynamics

To quantify heart-arterial system interaction, Otto Frank developed the first mathematical model that successfully related global systemic arterial system properties to aortic pulsatile pressure and flow (92). This early model described large arteries as a single compliant compartment distending and storing blood in systole. In diastole, the aortic valve closes, and the recoil of the large arteries propels blood continuously to the rest of the system. Although explicitly based on the assumption of conservation of mass, the model had an implicit assumption that pressures in the large arteries rise and fall simultaneously. As a result, all storage of blood is determined by the total arterial compliance (C_{tot}) and all resistance to blood flow is determined by the total peripheral resistance (R_{tot}) (77, 92). The resulting model predicts an exponential fall in pressure in diastole, which roughly approximates measured aortic diastolic pressures (72). The implicit assumption that pressures in the large arteries rise and fall simultaneously is equivalent to the assumption of infinite pulse wave velocity (77), or more generally,

infinite pulse wavelength. This assumption has been considered to be a limitation of 0-D model (3). Pulse pressures are directly related to only two parameters, R_{tot} and C_{tot}.

1.3 Spatially distributed large-scale realistic arterial system model

Transmission line descriptions of the arterial system were developed to address the inherent limitations of the Windkessel model. Based on linear approximations to the Navier-Stokes equation, this approach includes the effects of blood inertia, and arterial length arises as an explicit parameter (136). The resulting equation of motion is capable of representing phenomenon involving pulse wave length, i.e., the pressure pulse consists of waves traveling in both forward and backward directions (11, 132). Pulses generated at the heart travel to the periphery, and are reflected whereever there is a change in the local impedance, which occur at bifurcations or in regions where the geometry or stiffness of vessels change (47). Based on this description, numerous large-scale distributed arterial system models were developed to capture the realistic topology of the mammalian systemic arterial tree. The model proposed by Westerhof et al. (128, 129) relates aortic input impedance to the radii, lengths and compliances of 121 arterial segments, and has formed the basis for several models with increasing levels of complexity (5, 83, 99). This model yields a realistic root aortic pressure when coupled with a realistic root aortic flow, and has helped establish that the arterial system has significant pulse wave reflection (128, 129). It is clear from the discussion above, unlike classical Windkessel, this description takes lengths of the arterial segments into account. Thus the description is considered as 1-D model. A 1:1 scale hydraulic model (100) was implemented to mimic the 1-D distributed model (129) and found to predict pressure and flow pulses accurately.

With such 1-D models, local pulse pressure is explicitly related to the spatial distribution of compliance (e.g., the relative compliances of mother and daughter vessels at a bifurcation), and not total arterial compliance as a Windkessel.

1.4 Modeling perspectives

Over the years, numerous models have been developed to characterize the human arterial system. From a modeling perspective, models can be classified as those without spatial information (0-D), with axial length of the arteries in the network (1-D), and up to the most realistic geometries (3-D). Essentially, 1-D models can include the complexity of inertial effects missing from 0-D models. The transition from 0-D to 1-D was achieved analytically, which required rigorous effort with difficult mathematical manipulations, starting with ad-hoc approaches (77), linearization of Navier-Stokes equations (134), finally hitting its pinnacle with Womersley solution (35, 135, 136). With the advancement of computational capabilities, 2-D and 3-D models became much easier to implement and are now quite common. We are in an era when 3-D patient-specific models are overtaking 2-D models (23). However, 0-D and 1-D models do have analytical solutions. They can provide level of insight and understanding between the cause and effect that is difficult to recover from 2-D and 3-D models. It is obvious that reality is best captured in 3-D models with accurate boundary conditions. However, 1-D models can be more than adequate when only pressure and flow are needed (100).

1.5 N-element Windkessel models

Despite evolution of spatially-distributed transmission models, simpler models with very few parameters are still in high demand. Having arterial lengths, radii and compliances, the transmission models can provide solution to the "forward" problem, i.e., given all the known parameters, it can predict the pressure and flow in the vessel segments. However, it fails to provide a solution to the "inverse" problem, i.e., having a measured pressure and flow and inferring mechanical properties of the vessel segments. It is not practical to extract meaningful information for over 100 vessel segments from one pressure and flow pulse. Later it was found that there is an infinite number of solutions for such "inverse" problems, e.g., similar pressure and flow pulses can be achieved if the arterial segments are small and compliant or long and stiff (21, 89). Therefore, investigators have used lumped models (which have a limited number of parameters and no spatial information) that can be fit to measured data to derive parameter values. This is used in particular to understand how the parameters, e.g., C_{tot} and R_{tot} are altered in situations like isolated systolic hypertension or after a particular intervention (32, 34, 130). The classical (2-element) Windkessel model is the simplest version which can be fitted to data (106). Numerous models have been reported in the literature with 1) an extended number of lumped elements, 2) combinations of lumped elements and one or two uniform tubes, and 3) introduction of non-linear (i.e., pressure-dependent) compliance.

Most notable among the first group of lumped-element models is the 3-element Windkessel proposed by Westerhof (130). This model has an additional element representing the characteristic impedance of the first section of the aorta. This model fell

short in predicting pressure and flow, when true total arterial compliance and characteristic impedance is used (106). When fitted to the data, this model overestimates C_{tot} (106). Goldwyn et al. introduced proximal and distal compliance to account the oscillation in diastolic pressure pulse (34). Canty et al. introduced viscoelastic compliance in the Windkessel (22).

In the second group, investigators used family of tubes terminated with resistances to introduce pulse wave propagation and reflection and (117). Later, elastic (120) and geometric tapering (127) were added, which led to unrealistic peaks in the frequency domain. Burattini et al. terminated the T-tube model with a 3-element Windkessel model (18).

The third group of models came with adding non-linearity of element properties. Liu et al. introduced pressure-dependent compliance (53) in a classical Windkessel. However, Li et al. proposed compliance of 3-element Windkessel as an exponential function of pressure (50).

N-element Windkessel or Windkessel-tube models fill a niche between the classical Windkessel and transmission model. It is clear from the previous paragraphs that proposed n-element Windkessel models were used either to describe measured data empirically to estimate properties of the arterial system. Increased number of elements can offer better fit to the data but may fail to achieve the optimal balance of the number of unknown to the goodness of fit (1). The Akaike Information Criterion (AIC) provides the justification of number of unknown parameters (1).

Sometimes, even when the number of parameters are justified, the physiological interpretation is not well defined. For instance, the 4-element model has brought

controversy of placing the total arterial inertance in series or parallel, as each combination falls short describing the arterial system (17, 101). The 5-element Windkessel has a term that could represent either a venous compliance (28) or distal compliance (34). The physiological relevance of the elements in a model with more than 5 elements is even more ambiguous.

An n-element Windkessel can always be fit to data—describing both frequency and time domains (assuming a particular input flow). They are very useful for terminating a tube, or predicting heart-arterial system interaction (5). However, they are rarely used for predictive purposes.

1.6 Windkessel as a predictive model

Over the years, the Windkessel model has been used to estimate arterial system parameters empirically by adjusting the parameter values (e.g., C_{tot}) to fit the experimental data. This method will allow this model to be *descriptive*, empirically describing the data well by minimizing the deviation between the model and the data. However, the Windkessel has been recently used as the basis of a completely different approach (83, 84). In particular, the Windkessel model was used as a *predictive* model, given known values of C_{tot} and R_{tot}. Pressure was predicted for an arterial system behaving like a Windkessel. The resulting output of the model was the "Windkessel approximation"—the aortic pressure and input impedance expected if pulse wavelength is long enough to cause the arterial system to degenerate into a Windkessel. This predicted pressure pulse from Windkessel model will be used to quantify the similarity of a real arterial system from a Windkessel and will be termed as "Windkesselness". To quantify

the amount of similarity, the aortic pressure pulse of an arterial system will be compared (by determining correlation coefficient, r^2) with that of its 2-element Windkessel equivalwent model. This approach made it possible, not so much that 1-D model can degenerate into a 0-D model, but instead, that the arterial system itself can degenerate into a simple Windkessel. This methodology is illustrated graphically in figure A-2.

1.7 Isolated systolic hypertension

The example of isolated systolic hypertension (ISH), a condition where systolic pressure is elevated and diastolic pressure remains normal, exposes a conflict between the approaches to determining arterial system properties from measured aortic pressure and flow (i.e., the "inverse problem"). One model has focused on the distributed nature of the arterial system. Assuming a spatially-distributed transmission line model, some studies suggested that changes in the magnitude of pulse wave reflection from the periphery and the timing of the return of the reflected wave (74, 131) are responsible for ISH. The other model focused on the storage properties of the arterial system. Assuming a lumped Windkessel model, these studies suggested that decreased total arterial compliance (9) or peripheral compliance (8) are responsible for ISH.

Although both models clearly implicate changes in compliance in the manifestation of ISH, they clearly identified such changes as either regional or global. It is interesting to note that McVeigh et al. (59) used a modified 4-element Windkessel to show that distal compliance decreases, but proximal compliance increases in hypertension, i.e., an impedance mismatch causes the higher pulse pressure. Similarly, several approaches in the transmission model have indicated that small changes in

compliance ratios at bifurcations is the cause of impedance mismatch and thus altered pulse pressure (72). In fact, it is possible to decrease compliances of all three vessels (mother and daughters) at a bifurcation, yet maintain impedance matching. In each of these cases, the transmission models implicate the changes in regional compliances, and not total compliance in increased aortic pulse pressure.

On the other hand, the Windkessel offers a simple interpretation by implicating only changes in total arterial compliance in the high pulse pressure in ISH (72). The fact that the arterial system may be approximated by a 0-D model, and thus the transmission model loses its 1-D nature did not occur to investigators until very recently (83, 84). Therefore, no one using 1-D transmission models had previously shown that C_{tot} can be the primary determinant of pulse pressure, or that local changes in compliance can have little or no effect. In essence, both models have identified different changes in parameters with ISH to support their claims. The conclusions drawn by each model are directly related to the parameters that show up explicitly in the equations used (i.e., C_{tot} for Windkessel model, and local reflection coefficient for transmission model).

1.8 Separation of forward and reflected waves and their interpretation

At any location of the arterial system, the pressure and flow waves are composed of forward waves propagating from the beating heart and reflected waves from the sites of reflection. Pulse wave reflection has been implicated in several cardiovascular diseases. Therefore, it was necessary to address its affect on pulse pressure morphology. Wave separation analysis is commonly used to separate forward (P_f) and reflected (P_r) pressures from measured pressure (P) and flow (Q) waveforms. It can be performed in

both time and frequency domain (40, 49, 132). Time-domain analysis, shown in the following equations, deserves particular attention since it has brought considerable controversy interpreting the role of reflection.

$$P_f = \frac{P + Q.Z_o}{2} \qquad (1a)$$

$$P_r = \frac{P - Q.Z_o}{2} \qquad (1b)$$

Here, Z_o is characteristic impedance, the input impedance in the absence of reflection (16, 46, 49, 96, 132). Following this time-domain methodology and keeping the mean values in, the reflected pressure wave is always positive and adds to the forward pressure. Although this became popular, it was later challenged with the insight that pulse wave propagation and reflection are completely oscillatory phenomena (11, 12). Therefore, the analysis should be performed with only the oscillatory parts of the pressure and flow pulses, i.e., P and Q with mean values subtracted (11, 12). The resulting forward and reflected pressure waves swing both positive and negative. Thus, the reflected wave will raise pressure at one instant, and will lower pressure at another instant. Forward and reflected pressure waves calculated from both methods have identical shapes. The former method often leads to the interpretation that pulse wave reflection can only add constructively with the forward wave, and thus reflection always increases pulse pressure (72-74, 77, 81). As a consequence, Westerhof and O'Rourke suggested (131) that the rational approach to treating isolated systolic hypertension is to decrease the magnitude of reflection, a stance that has become common among quantitative hemodynamicists.

1.9 Pressure pulse morphology and concept of the Augmentation Index

Although pulse wave reflection is slowly becoming accepted by investigators as a clinically-relevant variable (65, 73, 95, 97), calculation of the reflected wave via wave separation analysis requires measurement of both aortic pressure and flow (132). In order to characterize the systemic arterial system with measured aortic pressure alone, Murgo et al. (69) classified pressure morphologies into three different types (*A, B* and *C*). *Type A* morphology has drawn most attention among clinical investigators (43, 63, 71), and usually manifests among the individuals of age 45 to 65. *Type A* morphology has a well-defined inflection point in aortic pressure waveform in late systole. Murgo et al. and subsequent investigators (43, 69, 72) have attributed this inflection point to the arrival of a reflected pressure wave that "augments" the pressure. This augmented pressure is believed to be so prominent in this group because it results from both a general increase in reflection as well as an early return from the periphery (131). *Type B* morphology, usually manifests between the age of 30 and 40, has a similar inflection point in the late systole, but exhibits less "augmentation", presumably because the magnitude of reflection generated from primary reflection sites is lower. *Type C* morphology manifests in young, healthy subjects, and exhibits the least "augmentation". Furthermore, the inflection point occurs later in systole or even in diastole, presumably because the pulse wave velocity is lower or the primary site of reflections are further from the heart (65).

Type D morphology was introduced by Nichols et al. (71, 74) to describe the pressure morphology of subjects 65 and older with hypertension, which is characterized by the lack of a discernable inflection point. To quantify these pressure pulse morphologies with a simple index for clinical use, the Augmentation Index was

introduced by Kelly et al. (43). Expressed as a ratio of the "augmented pressure" to pulse pressure, the Augmentation Index was found correlated with age (43), atherosclerosis (4), hypertension (20), heart failure (116), and end-stage renal disease (54).

1.10 Difficulties evaluating and interpreting the Augmentation Index

Despite the growing adoption of the Augmentation Index, persistent questions have arisen in its calculation and interpretation. First, Segers et al. (96) found that analysis of the pressure wave alone yielded inaccurate estimates of when the reflected wave arrives. Second, *Type D* pressure morphology does not exhibit the inflection point common to morphology *Types A-C* (74). Attempts to identify inflection points by taking second, third, or even fourth derivatives of the pressure pulse with *Type D* morphology remains problematic (72). Third, although pulse wave reflection has been shown to consistently increase with age (131), the Augmentation Index has been reported to decrease above a certain age (29). Fourth, reflection sites have been reported to shift away from the heart with age, even though the inflection point in pressure occurs earlier in systole, which is interpreted as an earlier arrival of the reflected wave (65). Although problems implementing the augmentation index have been identified, the four fundamental assumptions listed on section 1 (heading 1.1, paragraph 2) concerning the conventional view of pressure pulse reflection have not yet been challenged.

1.11 Axial-flow LVADs present unique opportunity

Axial-flow left-ventricular assist devices (LVADs) represent a new advance in technology to provide support for patients suffering from heart failure, one of the most common causes of mortality in developed countries (27, 30, 82, 103). Whereas "second-generation" LVADs provide a pulsatile flow by mimicking the periodic contraction and relaxation of the ventricle, these "third-generation" LVADs have an impellor that rotates at 2000-5500 rpm (38, 55). Axial-flow LVADs therefore provide a relatively steady flow as they pump blood from the left ventricle to the aorta, bypassing the aortic valve (27, 82, 121, 123). When LVADs are tuned properly, the heart continues to contract and expel blood through the aortic valve, ensuring that arterial pressure nonetheless remains pulsatile (76, 123). The novel design of axial-flow LVADs allows them to be much more efficient and smaller than pulsatile LVADs. Furthermore, clever device design and the rapid evolution of clinical practices have solved many of the problems plaguing former generations of LVADs, such as mechanical failure, hemolysis, thrombo-embolism, leakage, and potential for infection (2, 41, 44, 62). Taken together, these advances are expanding the use of LVADs from a temporary bridge-to-transplant available only to males with large chest cavities (82), (60) to "destination therapy" available to small women or even infants (27, 57, 82). The very success of axial flow LVADs, however, has brought a new set of challenges to the forefront.

1.12 LVAD-heart-arterial system interaction presents challenges for axial-flow LVADs

Four distinct challenges have arisen that impact further advances on safety, effectiveness, and expanded use of axial-flow LVADs. First, if ventricular failure is particularly severe or the LVAD removes blood from the ventricle too quickly, the ventricular pressure may no longer be able to rise above aortic pressure. This causes the aortic valve to remain shut throughout the cardiac cycle, increasing the potential for thrombus formation in the aortic root (124). Second, if the LVAD speed is set too low, aortic pressure may transiently rise above the pressure gradient generated by the LVAD. Blood thus can regurgitate through the pump, inappropriately loading the ventricle during diastole (25, 110, 126). Third, if the LVAD removes blood from the ventricle faster than it can fill from venous return, it can cause ventricular collapse, a particularly painful experience (76), (41). Fourth, to accommodate changes in physical activity, the LVAD speed would have to be modulated by an automatic, stable, adaptive controller. To ensure optimal control and to adjust LVAD speed to avoid regurgitation, persistent aortic valve closure, or ventricular collapse, the algorithm would have to have predictive capabilities (41, 58, 125, 126). These are not four independent challenges of device design, but a single problem of applied physiology: the behavior arising from ventricular-arterial interaction is highly nonlinear, complex, and difficult to predict quantitatively.

1.13 Need to supplement conventional tools to study the complex interaction

Computational fluid dynamics modeling is a useful tool to study the interaction of axial-flow LVADs and blood, and has led to the design of LVADs that minimize

hemolysis (137) and thrombus formation (15, 64). However, the dual requirement of precise boundary conditions and extensive computational resources limits simulations to a small section of a "representative" cardiovascular system. Closed-loop mock circulations are therefore a useful tool, since they can be set up to mimic an entire human cardiovascular system (102), as well as validate computational fluid dynamics predictions (102) and test LVAD prototypes (102, 122). It is difficult, however, to empirically characterize LVAD performance as a function of more than a few parameters. Testing of LVADs in canine, ovine, porcine or bovine animal models is of course required (31, 42, 55, 61, 93). The high cost of animal experiments and the inability to alter more than a few variables at a time, however, conspire to limit the usefulness of animal models as a development tool. Although all three tools are *necessary* for LVAD design and testing, they have not been *sufficient* to predict changes in LVAD performance with changes in ventricular filling, ventricular contractility, heart rate, peripheral resistance, or total arterial compliance.

1.14 Mathematical models of heart-arterial interaction

The analytical tools conventionally used to predict the cardiac output were first characterized in a time before heart-arterial interaction could be measured in animals or simulated by computer. Otto Frank (1895) took the first step by developing the classical (2-element) Windkessel (92). This arterial system model lumped the large conductance vessels into a single compliant chamber which distends to store blood in systole and recoils in diastole. Similarly, the peripheral vessels were lumped into a single term characterizing the resistance to flow of blood out of the chamber. The second step was

taken by Suga et al., who characterized the contractile properties of ventricles as a ratio of instantaneous ventricular pressure and volume (114). Extending the use of the end-systolic pressure-volume relationship (ESPVR) as an index of the ventricular contractility, this pressure-volume ratio was assumed to vary with time (112). It only took a few years before this "time-varying elastance" model was coupled with variations of the classical Windkessel model (105). The final step was taken by Sunagawa et al. (115) who combined these two model equations and developed an analytical (i.e., algebraic) solution. Though this solution was elegant and indicated how changes in arterial and ventricular properties affected cardiac output, it was criticized for assuming a simple Windkessel model (24).

2. DISSERTATION OBJECTIVES

The concept of pulse wave reflection was originally developed to explain arterial pressure-flow relationship and thus characterize heart-arterial interaction. However, the insight that pulses generated at the heart are reflected back from peripheral sites formed a basis for understanding several cardiovascular patho-physiological conditions. The Windkessel model describes the arterial system as a compliant chamber that distends and stores blood, and relates pulse pressure to total peripheral resistance (R_{tot}) and total arterial compliance (C_{tot}). Inherent in this 0-D description is that arterial pulse wavelengths are *infinite*. The Transmission model, having a *finite* pulse wavelength, describes the arterial system as a network of vessels with axial lengths that transmits pulses, and relates pulse pressure to the magnitude, timing and sites of pulse wave reflection. Limited by only two global properties and no spatial dependence, Windkessel description can implicate only global changes, e.g., change in C_{tot}, in the observed changes in pulse pressure. The transmission description implicates changes in local reflection for observed changes in pressure pulse. Therefore, the conclusions drawn by each model are directly related to the assumptions inherent in modeling approach, i.e., either it is change in global compliance or local reflection coefficient.

Although recent advances have provided much-needed insight, the Windkessel and transmission models have yet to be exploited to solve three interrelated problems. As discussed in the previous section, Windkessel will be used as a predictive model. First, the effect of total arterial compliance on aortic pulse pressure was not quantified in terms of deviation from one model to another. Second, although two critical cardiovascular

parameters (heart rate and arterial radii) affect wave length, they also affect characteristic impedance and local pulse wave reflection. It was not addressed how these two sets of parameters can also cause an arterial system to degenerate into a classical Windkessel. Third, the mechanical properties that are responsible for increased pulse pressure in isolated systolic hypertension were not identified, leading to a necessary step in developing a rational basis for the treatment of hypertension. The present work will address each of these omissions.

Since pulse wave reflection has become a clinically relevant variable, investigators have attempted to use the morphology of pressure pulses to infer effects of pulse wave reflection. Pulse morphologies of elderly subjects exhibit distinctive inflection points during systole, conventionally believed to result from the reflected wave adding constructively with the forward wave. The speed at which pressure pulses travel increases with age and hypertension is ascribed primarily to decreases in aortic arterial compliance. This increase in pulse wave velocity is believed to explain why the peak of the reflected wave arrives earlier in the contraction cycle, when the ventricle is still ejecting. Furthermore, the magnitude of the reflected wave also increases with age and hypertension. This phenomenon has been attributed to a loss of the "impedance matching" at bifurcations that normally allows pulses to be transmitted with very little reflection. Taken together, it has been posited that the reflected wave increases pulse pressure and the mechanical load of the heart. These interpretations, as mentioned earlier in section 1, are based on four fundamental assumptions: 1) pulse wave reflection always augments pressure, 2) an increase in aortic pulse wave velocity causes a commensurate shift in the arrival of the reflected wave, 3) the time of arrival of the reflected wave

depends on the distance to the sites of major reflection, and 4) increases in the magnitude of local reflections increase the magnitude of the reflected wave reaching the heart. The present work challenges these basic assumptions.

There has been significant success in describing the complex interaction of the heart and systemic arterial system. The recent practice of incorporating ventricular assist devices to treat cardiac failure poses an additional complexity. The variables influencing the interaction either cannot be measured or controlled, and the generality of the results gained from numerical simulation are limited. Though mock circulations, animal experimentation and computational fluid dynamics are excellent tools, they are not sufficient to describe the heart-LVAD-arterial system interaction. At the same time, quantitatively relating the performance of an axial-flow LVAD to arterial system properties depends on whether the pulse propagation and reflection or Windkessel function determines pulsatile pressure in the ascending aorta. Several distinct challenges have arisen that impact further advances on the safety, effectiveness, and expanded use of axial-flow LVADs. On the one hand, in case of severe ventricular failure, ventricular pressure may not be able to rise above aortic pressure as the LVAD removes blood from the ventricle too quickly. This leads to closure of aortic valve during systole and increases the potential for thrombus formation in the aortic root. On the other hand, if the LVAD speed is set too low, blood thus can regurgitate through the pump, inappropriately loading the ventricle during diastole. To accommodate changes in physical activity, the LVAD speed would have to be modulated by an automatic, stable, adaptive controller. To ensure optimal control and to adjust LVAD speed to avoid regurgitation, or persistent aortic valve closure, the algorithm would have to have predictive capabilities. These are

not four independent challenges of device design, but a single problem of applied physiology: the behavior arising from ventricular-arterial interaction is highly nonlinear, complex, and difficult to predict quantitatively.

The three main issues described in the previous three paragraphs are a manifestation of a single problem: there is a fundamental, unresolved debate as to the critical arterial system variables affecting pulsatile pressure. The central hypothesis of this dissertation is that the systemic arterial system degenerates into a classical (2-element) Windkessel as pulse wavelength increases in elderly and hypertensive. If true, total arterial compliance and total arterial resistance are the only important parameters effecting pulse pressure morphology, and the description of the arterial system becomes much more tractable for analytical characterization.

2.1 Objectives

2.1.1 Objective 1: Quantify Windkesselness in human systemic arterial system

Hypothesis: The systemic arterial system transforms into a simple Windkessel as pulse wavelength increases.

1. Specific Aim 1: Identify the hemodynamic parameters influencing to increase Windkesseness in the human arterial system using a mathematical approach.
2. Specific Aim 2: Experimentally determine alteration of Windkesseness due to aging.
3. Specific Aim 3: Determine which cardiovascular parameters affect pressure and flow during isolated systolic hypertension.

2.1.2 Objective 2: Reinterpretation of the Augmentation Index

Hypothesis: When systemic arterial system degenerates into a classical Windkessel, local reflection effects, e.g, changes in effective length, impedance mismatches at bifurcation and pulse wave velocity, become irrelevant.

1. Specific Aim 1: Calculate forward and reflected wave utilizing both less appropriate and more appropriate wave separation analysis for normotensive subjects of different ages.
2. Specific Aim 2: Propose a new technique to estimate pulse pressure augmentation by the reflected pressure wave.
3. Specific Aim 3: Determine the relevance of local reflection variables (e.g., effective length, sites of reflection) with hypertension.

2.1.3 Objective 3: Quantify heart-arterial-LVAD interaction

Hypothesis: Degeneration of systemic arterial tree into a classical Windkessel model allows first-order analytical approximation to adequately describe heart-arterial system-LVAD interaction.

1. Specific Aim 1: Derive an analytical formulation approximating mean pressure and flow as a function of heart, arterial system, and LVAD parameters
2. Specific Aim 2: Validate the analytical solution with a well-accepted distributed arterial system model.

3. Specific Aim 3: Determine which and how key cardiovascular properties affect LVAD performance

Section 3 will quantify the '*Windkesselness*' of the systemic arterial system. The large-scale realistic distributed model proposed by Westerhof et al. (129) and its classical 2-element Windkessel-equivalent model will be compared. The results will be then compared with previously-reported experimental data. To quantify the amount of deviation, the aortic pressure pulse of an arterial system will be compared (by determining correlation coefficient, r^2) with that of its 2-element Windkessel equivalent model. The r^2 value determines the "Windkesselness" of that arterial system. In the following sections, the pressure pulses under comparison will be considered similar when $r^2 \geq 0.99$.

Section 4 will address a popular non-invasive, yet controversial index for the effects of arterial stiffness, atherosclerosis, and hypertension—the augmentation index. Taking the notion from the previous section, it will cover the role of 'Windkesselness' in the augmentation index. Direct analysis of data, large-scale realistic distributed modeling and introduction of an index of true augmentation index will be covered.

Section 5 will apply the principle that an arterial system can transition to a classical Windkessel to address development of first-order approximation to describe the heart-arterial system-LVAD interaction. This work will extend the approximation of Sunagawa et al. (115) for heart-arterial system interaction to explain the interaction when a steady flow source is added. This section will also introduce an axial-flow LVAD into the large-scale arterial system model to validate the approximation and explore the effects of pulse wave reflection.

3. WINDKESSELNESS OF THE SYSTEMIC ARTERIAL SYSTEM

Two modeling approaches ascribe vascular disease states such as isolated systolic hypertension to fundamentally different arterial system properties. The Windkessel model describes the arterial system as a compliant chamber that distends and stores blood, and relates pulse pressure to total peripheral resistance (R_{tot}) and total arterial compliance (C_{tot}). The Transmission model, assuming a *finite* pulse wavelength, describes the arterial system as a network of vessels that transmits pulses, and relates pulse pressure to the magnitude, timing and sites of pulse wave reflection.

Although recent advances have provided much-needed insight, Windkessel and Transmission models has yet to be exploited to solve three interrelated problems. First, focusing on the frequency domain, Quick et al. (83, 84) did not quantify how changes in arterial compliance affect aortic pulse pressure. Second, focusing on compliance (85), they did not address how changes in two other critical cardiovascular properties (heart rate and arterial radii) can also cause an arterial system to degenerate into a Windkessel (83). Third, they did not identify the mechanical properties that are responsible for increased pulse pressure in ISH, a necessary step in developing a rational basis for the treatment of hypertension (131).

In this section, each of these three problems will be addressed by developing a novel approach to quantify how much an arterial system behaves like a classical Windkessel. Parameters affecting pulse wavelength will be systematically altered in a realistic, large-scale human arterial system model, and the resulting pressures will be compared to those assuming a classical (2-element) Windkessel with the same R_{tot} and

C_{tot}. Model results will be validated with analysis of representative human aortic pressure and flow waveforms reported in the literature (71).

3.1 Theory

3.1.1 Characterizing the arterial system independent of the heart with input impedance

Pulsatile pressure and flow depend not only on the arterial system, but also on the properties of the heart. Since the aortic pressure-flow relationship is generally linear, (84, 119), the concept of input impedance is typically invoked to characterize the arterial system independent of the heart (79). Whereas pulsatile pressure and flow are typically expressed in the time domain, the pulsatile load to the ventricle formed by the arterial system can be described by aortic input impedance (Z_{in}), the relationship of input pressure (P) to input flow (Q) expressed in the frequency (ω) domain (77).

$$Z_{in} = \frac{P(\omega)}{Q(\omega)} \tag{3.1}$$

3.1.2 Hemodynamic factors influencing input impedance

The relationship of input impedance to pulse wave propagation and reflection phenomena is briefly reviewed here. The arterial system at any particular location can be described mathematically as a compliant tube terminated by a load consisting of a branching arterial network. Z_{in} of a vascular bed depends on the characteristic impedance of the first artery (Z_o), its length (l), the pulse wavelength (λ), and the load at the end of

the vessel (Z_L). Taking into consideration the pulse reflection that occurs at the end of the tube results in a description of input impedance (12, 84).

$$Z_{in} = Z_o \frac{Z_L + Z_o + (Z_L - Z_o)e^{-4\pi j \frac{l}{\lambda}}}{Z_L + Z_o - (Z_L - Z_o)e^{-4\pi j \frac{l}{\lambda}}} \qquad (3.2)$$

Equation 3.2 completely describes input impedance in individual vessels, and can be applied to any vessel within a branching arterial network. Z_L, then, is the input impedance at the end of the vessel representing the load formed by the rest of the arterial tree.

3.1.3 Relationship of arterial mechanical properties to hemodynamic factors

Ultimately, the key factors affecting pulsatile phenomena—characteristic impedance and pulse wavelength—depend on mechanical properties of arteries as well as the blood. Two basic approaches have been used to derive this relationship. First, Noordergraaf (77, 78) took an ad hoc approach to arrive at equations of motion and continuity. Assuming that the axial pressure gradient in a vessel is equal to a pressure drop due to the inertia of a column of blood and viscous effects described by Poiseuille's Law, vessel inertance (L') and resistance (R') per unit length were characterized. Assuming a vessel with linear elasticity, vessel compliance per unit length (C') (i.e., the change in cross sectional area with change in pressure) was characterized. The resulting characterizations of R', L' and C' can alternatively be derived by a more rigorous approach based on linearizing the Navier-Stokes equation (77, 136). Briefly, all nonlinear and second-order terms (e.g., $\partial^2 v_z/\partial z^2$, $\partial^2 v_z/\partial r^2$) were neglected, as well as

rotational flows. However, viscous term remained with the lower order of the linearized equation. In larger vessels, this method yields equivalent values for L', R' and C' expressed in terms of blood density (ρ), vessel radius (r) and blood viscosity (μ) (77),

$$R' = \frac{8\mu}{\pi r^4} \qquad L' = \frac{\rho}{\pi r^2} \qquad C' = \frac{dA}{dP} \tag{3.3}$$

where A is the cross-sectional area, equal to πr^2. As a result, Z_o can be expressed as a function of ρ, μ, r and C' (77). In the larger arteries, viscous effects become negligible, and Z_o simplifies.

$$Z_o = \sqrt{\frac{j\omega L' + R'}{j\omega C'}} = \sqrt{\frac{j\omega \frac{\rho}{\pi r^2} + \frac{8\mu}{\pi r^4}}{j\omega C'}} \approx \sqrt{\frac{\rho}{\pi r^2 C'}} \tag{3.4}$$

The other parameter of importance in *Eq. 3.2* is the pulse wavelength (λ) which is a function of r, C', μ, ω and ρ. In larger vessels, the viscous effects become negligible, and the normalized wavelength of a pressure pulse at the heart rate (HR) simplifies. The ratio of wavelength (λ) to length (l) provided the information of how closely a system is behaving like a Windkessel.

$$\frac{\lambda}{l} = \frac{j\omega}{HR \cdot l\sqrt{j\omega C'\left(j\omega L' + R'\right)}} = \frac{j\omega}{HR \cdot l\sqrt{j\omega C'\left(j\omega \frac{\rho}{\pi r^2} + \frac{8\mu}{\pi r^4}\right)}} \approx \frac{\sqrt{\pi r^2 / \rho C'}}{HR \cdot l} \tag{3.5}$$

Equations 3.4 and *3.5* are used to describe the characteristic impedance and pulse wavelength in the large arteries of mammals (12, 77, 89, 132).

3.1.4 Windkessel arterial system model

The Windkessel model is much simpler than the Transmission description described above, because pressure and flow are assumed to vary slowly enough to make inertial effects negligible. As a corollary, pulses are assumed to have an infinitely long wavelength, which leads to simultaneous rise and fall of pressure within the arterial system. The Windkessel input impedance (Z_w) is a function of total arterial compliance (C_{tot}), total peripheral resistance (R_{tot}), and frequency (ω).

$$Z_W = \frac{R_{tot}}{1 + j\omega R_{tot} C_{tot}} \qquad (3.6)$$

Quick et al. (83-85, 87) illustrated both theoretically and experimentally that the arterial system degenerates into a Windkessel at low frequencies (either low frequency components or lower HR). This is a special case where the wavelength (*Eq. 3.5*) is long, as assumed by the Windkessel model. However, *Eq. 3.5* indicates that the changes in any of three parameters (*HR*, *C′*, *r*) could increase pulse wavelength.

3.1.5 Distributed arterial system model

The arterial system model used in the present work consists of 121 major arterial segments representing the large conductance vessels of the human systemic arterial system. The vascular parameters characterizing each vessel segment (*r*, *C′*, *L*) were first published by Westerhof et al. (128, 129). Using the transmission line equations described above, vessel inertance, resistance, and compliance per unit length were calculated (*Eq. 3.3*). These hemodynamic values were then used to characterize the pressure-flow

relationships in the 121 vessel segments. The proximal end of this large-scale model starts from the root of the ascending aorta and terminates with resistive elements in the periphery. Because the resistances in the 121 vessel segments were very small, almost all resistance in the system resided in these terminal resistances. Any changes in the radii of these conducting arterial segments therefore have negligible effects on mean pressure. Comparisons to later measurements of systemic arterial compliance (90) led Stergiopulos et al. (106) to suggest that the original model compliances were much too low to represent normal human values. Like models reported previously (83, 88, 107), we thus increased all of the original arterial segment compliances of the Westerhof model by 50% to represent the normal or "control" case. The input to this large-scale model was assumed to be a typical root aortic flow pulse of a healthy human at rest (Fig. A-2) originally reported elsewhere (106). It has a period of 1 second, a peak flow of 480 ml/sec, and a mean value of 83.33 ml/sec. Because the input flow was experimentally derived and included measurement error, there were very small oscillations in flow throughout diastole. The output of the model was input impedance and root aortic pressure (Fig. A-2A).

3.1.6 Predicting pressure and flow in Windkessel model

The same flow pulse is used as an input for the classical (two-element) Windkessel model (Fig. A-2B). Total arterial compliance (C_{tot}) for the Windkessel model was taken as the sum of all the compliances of the distributed model. Total arterial resistance (R_{tot}) for this model was set to match the resistance calculated from the average pressure and flow at the ascending aorta of the distributed model. The output of the

model is the Windkessel approximation—the aortic pressure and input impedance expected if pulse wavelength is long enough to cause the arterial system to degenerate into a Windkessel.

3.1.7 Comparison of the realistic distributed model with the Windkessel approximation

The pressure and input impedance of the distributed model were predicted for different values of *HR*, *C′*, and *r*. In order to increase pulse wavelengths 50% above normal values, *HR*, *C′*, and *r* were changed different amounts, given by *Eq. 3.5*. For the first case, *HR* was decreased by 33.3% to 40 beats/min. This was accomplished by scaling the time axis of aortic flow in Fig. A-2. For the second case, compliance of each arterial segment (*C′*) of the distributed model was reduced by 55.5%. For the third case, the radii of the arterial segments (*r*) were increased by 50%. In each case, total peripheral resistance was kept constant. For comparison purposes, total peripheral resistance and total arterial compliance of the distributed system for each case mentioned above (i.e., with altered values of *HR*, *C′* and *r*) were assumed for a classical two-element Windkessel model. The root aortic flow was kept same as the control case. Predicted pressure and input impedance of both distributed and Windkessel models were plotted on the same graphs.

3.1.8 Comparison of human data with the Windkessel approximation

Nichols et al. reported a substantial change in aortic pressure waveforms and input impedance with age (71). For comparison purposes, we digitized the reported pressures and flows for two extremes of age. The input impedance was then calculated with *Eq. 3.1* after pressure and flow were transformed into the frequency domain using the Fast Fourier Transform (FFT) (26). Total arterial compliance was estimated for both cases using the technique described in Quick et al. (83). Briefly, the apparent compliance was calculated from input pressure and flow, and the lowest frequency available was taken as the best estimate of C_{tot}. Total peripheral resistance was estimated by dividing average pressure by average flow. In this case, measured pressure and flow data are used in place of the Distributed arterial system model in Fig. A-2A. The input impedance of a Windkessel with the same C_{tot} and R_{tot} was predicted, as well as the pressure resulting from this Windkessel given the same measured input flow (Fig. A-2B). The predicted Windkessel input impedance and the pressure waveform were then graphed with the experimental data (17).

3.1.9 Quantifying the deviation of distributed model and Windkessel pressures

To quantify the deviation of the Windkessel model from the realistic Distributed model, a simple correlation coefficient was calculated. These models were considered similar when r^2=0.99 and difference in pulse pressure was less than 3 mmHg, signifying the degeneration of the arterial system into a classical Windkessel.

Figure A-2 illustrates the pressures resulting from inputting a measured human aortic flow into the distributed arterial system model (Fig. A-2A) and into the classical Windkessel (Fig. A-2B). Only if diastolic flow is exactly zero will diastolic pressure predicted from the Windkessel fall exponentially. The experimentally measured flow used as an input for both the Distributed and Windkessel models (106). Deviation of between the pressure pulses predicted from each model was then calculated with correlation coefficient (r^2).

3.2 Results

There was considerable deviation between the pressures predicted from the 0-D and 1-D models, particularly in systole. Figures A-3 *A* and *B* compare pressures and input impedances of the Distributed model (points) with those of a classical (two-element) Windkessel model (solid line) under normal physiological conditions. The correlation coefficient (r^2) was 0.95 for predicted pressures. For the first five (0-4) harmonics, mean error for input impedance was 28.63%. The deviation was higher above the fifth harmonic. These results serve as baseline for comparing the three cases described below.

In order to change wavelength (*Eq. 3.5*), heart rate, compliances and radii of the conductance vessels of the distributed model was altered one at a time. Figures A-3*C* and *D* illustrate pressures and input impedances from both models with a lower heart rate. A 33.3% decrease in *HR* yielded an increase in pulse wavelengths of 50%. Pulse pressures did not exhibit much deviation (r^2=0.99). Figures 2*E* and *F* illustrate the pressures and input impedances from both models with decreased compliance. A 55.5% decrease in compliance yielded an increase in pulse wavelengths of 50%. The pressure pulses were

highly correlated (r^2=0.99). Figures 2*G* and *H* illustrate that the correlation of pressures (r^2=0.99) increased when radii were increased in the realistic Distributed model. A 50% increase in radius yielded an increase in pulse wavelengths of 50%. Pressures in diastole also exhibited little deviation. In each case, the results from the Distributed model were more similar to the Windkessel model than the baseline cases in Fig. A-3. Input impedances, for first five (0-4) harmonics, exhibited smaller deviation (9.09% for lower HR, 7.87% for decreased compliances, and 9.64% for increased radii) from the control case. In all three cases, the deviation was higher above the fifth harmonic.

Measured pressure from normotensive young (28 years old) and elderly (68 years old) subjects were compared with those of Windkessel-equivalent pressures. Figures A-4*A* and *B* illustrate measured pressures and input impedances originally reported by Nichols et al. (71) (Fig. A-4). For the 28 year old subject, R_{tot} was estimated to be 0.66 mmHg/ml/sec and C_{tot} was estimated to be 2.20 ml/mmHg. The pressures predicted assuming a Windkessel with the same values of R_{tot} and C_{tot} (lines, Figs. A-4A and B) approximated (r^2=0.93) the measured pressure (points, Figs. A-4A and B). The mean error for first five (0-4) harmonics of input impedance was 73.45%. For the 68 year old subject, R_{tot} was estimated to be 1.08 mmHg/ml/sec and C_{tot} was estimated to be 0.96 ml/mmHg. The pressure predicted assuming a Windkessel with the same R_{tot} and C_{tot} (lines, Figs. A-4C and D) closely approximated (r^2=0.99) the measured pressure (points, Figs. A-4C and D). The mean error for first five (0-4) harmonics of input impedance was 12.48%. In both cases, deviation was higher above the fifth harmonics. The older subject exhibited less deviation between the measured data and the model results indicating degeneration into a classical Windkessel (r^2 = 0.93 vs. r^2 = 0.99).

Windkesselness of an arterial system increased with lower heart rate, lower compliance, and increased radii as indicated by higher correlation between pressures predicted from large scale arterial system model and the Windkessel model. Figure A-5 illustrates how rapidly the human systemic arterial system degenerates into a Windkessel with changes in heart rate, vascular compliances, and radii. In each case, the correlation between pressures resulting from the distributed and Windkessel models increased from r^2 value of 0.95 to 0.99 as pulse wavelengths increased 50% above normal values. Decreasing heart rate by 33.3%, decreasing arterial compliance by 55.5%, or increasing vessel radii by 50%, caused the correlation coefficient to increase to 0.99.

The relationship of pulse wavelengths to the resulting correlation coefficient was insensitive to the particular parameter that was altered. Figure A-6 describes the effect of increased pulse wavelength on the degeneration of the arterial system into a Windkessel. In each case (altered heart rate, vascular compliances and vessel radii) the correlation coefficient increased with increases in pulse wavelength.

3.3 Discussion

The work described in this section, illustrates with a realistic, large-scale model that the human systemic arterial system degenerates into a Windkessel when pulse wavelength increases as little as 50%. Wavelengths become long relative to the lengths of vessels when heart rate is low, vessel compliances are low, or vessel radii are large (*Eq. 3.5*). Although investigators have maintained that long wavelengths make an arterial system degenerate into a Windkessel (77), this postulate has never been tested, in part because of the inherent inability to independently alter heart rate, compliances and radii

experimentally. This is the first time that increases in wavelength have been shown to result in increased “Windkesselness”, both in terms of aortic pressure and input impedance (Figs. A-3, A-5 and A-6). Furthermore, the present work quantifies *how much* and *how quickly* an arterial system degenerates into a Windkessel within the physiological range of parameters.

3.1.1 Insight from case studies

These studies suggest that an arterial system can degenerate into a Windkessel when pulse wavelengths increase as little as 50% (Fig. A-6). These findings provide the insight to speculate about why pressure pulse morphology is altered in three physiologically-relevant cases.

Case I: Bradycardia: Both cardiac and non-cardiac abnormalities can lower heart rate to very low levels. With bradycardia, heart rate drops to a range of 30 to 50 beats per minute. If mean arterial pressure is maintained, pressure-dependent vascular wall properties would remain normal. In this case, the model predicts pulse wavelengths would increase by a factor of 1.5, and the arterial system will act more like a Windkessel, e.g., the diastolic pressure would fall exponentially (Fig. A-3C), and the input impedance would fall monotonically (Fig. A-3D). Indeed, the error between the distributed system and Windkessel approximation decreases as heart rate falls below 30 beats/min (Fig. A-5A). These model results are consistent with the exponential decrease in pressure in diastole reported in the literature (67), and therefore the hemodynamic changes reported with bradycardia can be attributed to increased wavelength and therefore increased “Windkesselness”.

Case II: Exercise-induced hypertension: When healthy individuals exercise, their heart rate increases to provide the necessary increase in cardiac output to meet the higher metabolic demand. In response to the attending increase in mean arterial pressure, there are minor increases in radii, and rather substantial decreases in (pressure-dependent) compliances of the conductance arteries (70). Interestingly, compliances and heart rate can change significantly, but may balance and result in relatively small change in pulse wavelength, as suggested in *Eq. 3.5.* If this is the case, system properties other than C_{tot} and R_{tot} (e.g., distance to primary sites of reflection) could play a significant role in determining pulse pressure, and diastolic pressures would not fall exponentially, nor would input impedance fall monotonically. The present work provides the methodology that could test this hypothesis.

Case III: Age-related changes in arterial structure: As humans age, there is a tendency for pulse pressure to increase, even when both heart rate and mean pressures remain normal. In this case, the aging process causes changes to the arterial wall composition (72), leading to both significantly decreased compliances and increased radii of the large conductance vessels. This causes pulse wavelength to increase (*Eq. 3.5*). In this case, diastolic pressure falls exponentially, and input impedance falls monotonically, as expected for a Windkessel. The present work provides insight for further study of this hypothesis from the perspectives of pulse wave reflection.

3.3.2 Identifying the causes of isolated systolic hypertension

These case studies provide an essential insight into the interaction of heart rate, arterial compliances and radii in normal individuals: changes in parameters in normal

conditions tend to balance and keep wavelength constant (*Eq. 3.5*), that is, as heart rate increases, the attendant increase in mean pressure causes compliances and redii to decrease. This suggests a homeostatic principle which acts to moderate pulse pressure. It is interesting to note that if this homeostatic principle is violated (e.g., mean pressure without an increase in heart rate as with hypertension) and pulse wavelength increases, the arterial system can begin to behave like a Windkessel. In this case, total arterial compliance (C_{tot}) and total peripheral resistance (R_{tot}) are the only arterial system mechanical properties that effect pressure and input impedance. Although increasing the radius of the vessels in the Westerhof model can cause it to degenerate into a Windkessel (Figs. A-3 G and H), the required increase (~50%) is not physiological. However, the reported changes in arterial compliance with ISH ranges from -57% to -75% (9, 45, 48, 138). Changing compliance in our model by the same amounts (-57% to -75%) resulted in r^2 = 0.995 to 0.998, indicating that this change in arterial compliance is enough to cause an arterial system to degenerate into a classical Windkessel. Similarly, estimated total arterial compliance of the older subject was 44% less than that of the younger subject (Fig. A-4). From model results (Figs. A-3E and F) and analysis of human data (Fig. A-4), it can be surmised that ISH is a manifestation of the degeneration of the systemic arterial system into a classical (2-element) Windkessel. Although changes in pulse pressure have been observed in patients with increased pulse wave velocity and the magnitude of the reflected wave (74, 131), the present study suggests that pulse pressure in ISH is directly related to only two global mechanical properties of the arterial system—total arterial compliance and total peripheral resistance.

4. REINTERPRETING THE AUGMENTATION INDEX

As pulses propagate from the heart through the arterial system, they are reflected from multiple sites back toward the heart. Changes in the timing, magnitude, and site of reflection have been identified as the major causes of isolated systolic hypertension (ISH). In support of this assertion, pulse morphologies exhibit distinctive inflection points during systole of elderly subjects, believed to result from the reflected wave adding constructively with the forward wave. This interpretation was based on the common belief that reflection always augments pulse pressure. The ratio of this "augmented pressure" to pulse pressure is given by the Augmentation Index (*AI*) (43) shown in Fig. A-7. Recent findings suggested, however, that reflection does not necessarily augment pulse pressure.

Using both classical Windkessel and spatially-distributed arterial system models, recent advancements have challenged the fundamental assumptions (mentioned in section 1.1) regarding pulse wave reflection. First, with model-dependent (14) and model-independent (84) approaches, it was shown that reflected pressure pulse waves can add destructively with forward pressure pulses in the aorta, therefore lowering systolic pressure. This effect has been (21, 49) often overlooked by investigators who did not remove mean values from pressure and flow before analyzing them into forward and reflected components, and therefore only predicted constructive adding of waves. Second, since the pulse wave can travel to the periphery and back approximately seven times within a single heartbeat, it was shown that the reflected pulse wave consists of a composite of multiple reflected and re-reflected waves (11). Increases in pulse wave

velocity not only affect the timing of the return of the composite reflected wave, but also of the composite forward wave. Third, it was shown theoretically that when pulse wave velocity increases, distances traveled to and from sites of reflection have a minimal to effect on aortic pressure (66, 89). Fourth, the Westerhof model and direct analysis of data was used to determine that the normal systemic arterial system is very similar (correlation coefficient r^2= 0.95) to the classical Windkessel (66). In fact, with decreasing compliance with age, the system degenerates into a classical Windkessel (66, 83). Taken together, these recent advances have challenged the fundamental assumptions about pulse wave reflection that undergird the interpretation of the Augmentation Index.

In this section, the physical basis of AI will be reinterpreted. Direct analysis of data, and realistic large scale mathematical modeling will be employed to explore the role of altered timing and sites of reflection in arterial systems with different degrees of stiffness.

4.1 Theory

4.1.1 Estimating forward and reflected waves

Pressure (*P*) and flow (*Q*) waveforms measured at any site in the arterial circulation is the result of a summation of a composite forward and reflected waves (designated by subscript *f* and *r* respectively).

$$P = P_f + P_r \qquad (4.1a)$$

$$Q = Q_f + Q_r \qquad (4.1\ b)$$

The measured pressure is typically analyzed into forward and reflected pressures using simple algorithms,

$$P_f = \frac{(P + Q.Z_o)}{2} \qquad (4.2a)$$

$$P_r = \frac{(P - Q.Z_o)}{2} \qquad (4.2b)$$

where, Z_o is the characteristic impedance, the input impedance in the absence of reflection (16, 46, 49, 96, 132). There are numerous ways to estimate Z_o from measured data, including time- and frequency domain methods (49, 56, 86). Direct substitution of measured pressure and flow into *Eq 4.2b* yields a reflected wave that always has positive values (49, 132). However, it has been reported (11, 86) that since pulse wave propagation and reflection are pulsatile phenomena, the mean values of pressure ($\bar{P}$) and flow ($\bar{Q}$) must be removed from *P* and *Q* before applying was separation analysis.

$$P_f = \frac{(P - \bar{P}) + (Q - \bar{Q}).Z_o}{2} \qquad (4.3a)$$

$$P_r = \frac{(P - \bar{P}) - (Q - \bar{Q}).Z_o}{2} \qquad (4.3b)$$

With this more appropriate application of wave separation analysis, the values of P_f and P_r average zero throughout a cardiac cycle, and reflected waves oscillate from negative to positive values (86).

4.1.2 Analysis of reported aortic pressure and flow data

Nichols et al. (71) reported a substantial change in aortic pressure waveforms and input impedance with age. From this seminal paper, we digitized the pressure and flow morphologies reported for 28, 52 and 68 year old subjects. C_{tot} was estimated from the apparent compliance (84) using a technique described in detail elsewhere (83). R_{tot} was estimated by dividing average pressure by average flow. Consistent with previous reports (86), Z_o was estimated for the root ascending aorta by averaging the magnitude of the aortic input impedance for harmonics 4-11. For illustrative purposes, the forward and reflected pressure waves resulting from applying *Eq. 4.2* (i.e, the less appropriate application of wave separation analysis), were compared to the forward and reflected waves resulting from applying *Eq. 4.3* (i.e., the more appropriate application).

4.1.3 Calculating the "Conventional Augmentation Index"

The Augmentation Index is conventionally calculated as the ratio of an "augmented" pressure, *AP*, and the pulse pressure, *PP* (43, 72, 74). The augmented pressure is assumed to be equal to the portion of the pressure pulse above the inflection point depicted in Fig. A-7A. This ratio will be denoted as the Conventional Augmentation index (*CAI*).

$$CAI = \frac{AP}{PP} \qquad (4.4)$$

4.1.4 Calculating a "True Augmentation Index"

Because reflected waves do not always add constructively a "true" index of pressure augmentation was developed, based on the more appropriate application of wave separation analysis (*Eq. 4.3*). In this case, pressures at peak systole and end-diastole are augmented by the values of the reflected wave P_r at the time of peak systole ($P_{r,s}$) and end-diastole ($P_{r,d}$). The True Augmentation Index (*TAI*) is therefore taken as the ratio of ($P_{r,s}$-$P_{r,d}$) to *PP* (Fig. A-7B).

$$TAI = \frac{(P_{r,s} - P_{r,d})}{PP} \qquad (4.5)$$

The values of $P_{r,s}$, $P_{r,d}$, *PP*, *TAI* and *CAI* were calculated for the 28, 52, and 68 year old subjects reported by Nichols et al. (71) and plotted.

4.1.5 Large-scale human arterial system model

The realistic, large-scale spatially-distributed arterial system model proposed by Westerhof et al. (129) was exploited to predict pulsatile pressure in the ascending aorta for subjects with different total arterial compliances. The model consisted of 121 arterial segments, each with different values of lengths, radii, and compliance. The original values compliances of each arterial segment was increased 50% in accordance with Stergiopulos et al. (106) to characterize the system of a young, normotensive person. The input to this large-scale model was assumed to be a typical root aortic flow pulse of a healthy human at rest, originally reported elsewhere (106). It has a peak flow of 480

ml/sec, a period of 1 second, and mean flow of 5 L/min. The output of the model was root aortic pressure.

4.1.6 The classical Windkessel to identify the role of compliance in pressure augmentation

Section 3 described a novel method to characterize the degree of "Windkesselness" (66) of an arterial system in order to determine if total arterial compliance (C_{tot}) and total peripheral resistance (R_{tot}) are primarily responsible for aortic pressure and flow (83-85, 89) (Fig. A-2). To analyze the "Windkesselness" of an experimental subject, the pressure predicted from the spatially distributed model in Fig. A-2A is replaced by measured pressure. The measured aortic pressure is then compared to the Windkessel with the same values of C_{tot} and R_{tot} derived experimental from the experimental subject.

4.1.7 Forward and reflected waves in a stiff arterial system

Numerous investigators have postulated that the magnitude of reflection generated at particular sites and the distance of reflection sites from the heart determine the overall timing and morphology of the reflected waves (69, 71, 73, 96). To test if this has a meaningful effect in relatively stiff arterial systems, the C_{tot} and R_{tot} of the Westerhof model were set equal to those of a 68 years old normotensive subject reported in the literature (71). Then to change local reflection sites and distance of reflections sites from the heart, this model was dramatically rearranged. The set of arterial segments of

upper and lower left limbs were detached from their original location and reattached to the right internal carotid artery and right vertebral artery (i.e., segments 26BG and 27A in (129), respectively). Finally, to remove any influence of vessel segment length and distance to local reflection sites, a classical Windkessel equivalent with the same C_{tot} and R_{tot} was constructed (Fig. A-2B). Each pressure was then subjected to the more appropriate application of wave separation analysis (*Eq. 4.3*) and the resulting forward and reflected waves were plotted.

4.1.8 Pressure morphology of severely hypertensive subject

To characterize whether *Type D* morphology arises from the degeneration of an arterial system into a classical Windkessel, pressure and flow pulses were digitized from a 68 year old subject reported Nichols et al. (71). R_{tot} and C_{tot} were estimated and pressure generated from the classical Windkessel equivalent was calculated (Fig. A-2B). Forward and reflected pressure waves were calculated from the experimental data and pressure from the classical Windkessel equivalent using the more appropriate procedure for wave separation analysis (*Eq. 4.3*) and plotted.

4.2 Results

Two different interpretations can be reached using the wave separation methods mentioned in subheading 4.1.1. Figure A-8 illustrates the forward and reflected pressure waveforms estimated from the less appropriate (*Eq. 4.2*) and the more appropriate (*Eq. 4. 3*) application of wave separation analysis for 28, 52 and 68 year old normotensive

subjects (71). The less appropriate method appears to indicate that reflected waves always have positive values (left side Fig. A-8), and the timing appears to support the concept that the arrival of the reflected wave is responsible for the inflection point in the 53 year old subject. The more appropriate method removes mean values of the reflected waves (right side, Fig. A-8), and illustrates that the reflected wave oscillated between positive and negative values. In fact, the early portion of the reflected wave actively decreases the aortic pressure at end-diastole. In the case of the 28 year old subject, the reflected wave has a negative value at the time of peak systole ($P_{r,s}$).

Appropriate use of wave separation analysis provides a net augmentation of pulse pressure, but only because the reflected wave decreases diastolic pressure. Figure A-9 compares the contribution of reflected wave at peak systole ($P_{r,s}$) and end-diastole ($P_{r,d}$), net augmented pressure ($P_{r,s}$-$P_{r,d}$), the True Augmentation Index (*TAI*) and the Conventional Augmentation Index (*CAI*) for 28, 52 and 68 year old normotensive subjects. Whereas the *CAI* increases monotonically with age, the TAI shows very little difference in the 52 and 68 year old. Furthermore, the reflected wave in the 28 year old actually decreases systolic pressure.

Introduction of new reflection sites in the models simulating the elderly does not have any effect on its pulse pressure morphology. Figures A-10A B and C illustrates the distributed model proposed by Westerhof et al. (129) with compliances changed to simulate a 68-year old subject, the same distributed model after rearrangement, and the classical Windkessel equivalent. Figure A-10D illustrates that the peak of the reflected wave occurs in systole, consistent with the experimental data illustrated in Fig. A-8. Figure A-10E illustrates that rearrangement of the distributed model to create new

reflection sites and change the distance to reflection sites has little effect on either forward or reflected waves. Figure A-10F illustrates the forward and reflected waves predicted if the system completely degenerated into a classical Windkessel. The fact that forward and reflected waves for the Windkessel equivalent are similar to Figs. A-10A and B indicates that the system had degenerated into a Windkessel, and thus vessel lengths and reflection from discrete sites do not influence aortic pressure. Thus, C_{tot} and R_{tot} are primarily responsible for the morphology and timing of the reflected wave.

To validate the model results in Fig. A-10, Fig.A-11A presents an illustrative pressure pulse of a severely hypertensive 61 year old subject originally reported by Nichols et al. (71) and the pressures calculated for the classical Windkessel equivalent (Fig. A-7B). Fig. A-11B illustrates the reflected wave calculated from the more appropriate procedure for wave separation analysis (*Eq. 4.3*) applied both to the reported pressure and the pressure from the classical Windkessel equivalent. Similarity of the waveforms indicates a high degree (e.g., r^2=0.99) of "Windkesselness" and is consistent with the model results in Fig. A-10.

4.3 Discussion

This work has demonstrated with a large-scale mathematical model of the human arterial system and direct analysis of experimental data that the conventional augmentation index severely misrepresents the effect of pulse wave reflection when arterial systems are very compliant or very stiff. On the one hand, when an arterial system is very compliant, pulse wave reflection can add destructively with the forward wave and *decrease* systolic pressure rather than augment it. On the other hand, when an

arterial system is very stiff, the system degenerates into a classical (2-element) Windkessel, and pulse wave reflection from discrete sites ceases to influence pulsatile pressure. Consistent with recent reports (11, 86) the present work therefore challenges the four fundamental assumptions described in the *Introduction* that undergird the interpretation of the Conventional Augmentation Index. 1) Reflection does not necessarily augment systolic pressure (Fig. A-9). 2) Increases in pulse wave velocity does not simply translate the reflected wave along the time axis (an amount equivalent to distance to major reflection sites divided by velocity), but instead changes the morphology of both composite forward and reflected waves (Fig. A-8). 3) Distances from the heart to reflection sites have little influence pulse pressure in stiff systems (Fig. A-10). 4) Pulsatile pressures in a stiff arterial system are governed primarily by total arterial compliance and total arterial resistance rather than the magnitude of reflection from discrete sites (Figs. A-10 and A-11). These weaknesses of the interpretation of the Conventional Augmentation Index could not be demonstrated by experimentation alone, since all the parameters affecting pulse wave reflection cannot be measured or manipulated experimentally. Instead, insight came from three accepted approaches based on fundamental principles of physics: large-scale, realistic modeling of a spatially-distributed arterial system (128, 129), analysis of the degree of degeneration into a classical Windkessel (13, 66, 87), and more appropriate application of wave separation analysis (*Eq. 4.3*) (11, 86).

4.3.1 Pulse wave reflection does not necessarily augment pressure

Methods for analyzing measured pressure pulses into the forward and reflected pressure waves (11, 51, 86) were revisited in the present work, since the less appropriate method (i.e., *Eq. 4.2*) directly impact the interpretation of the Conventional Augmentation Index. Pulse wave propagation and reflection is an oscillatory phenomenon, and thus wave separation analysis can only apply to the oscillatory part of pressure and flow (11)—there can be no reflection in a system with steady flow (86). The more appropriate method therefore requires removing mean components from pressure and flow before applying wave separation analysis (*Eq. 4.3*) (11, 86). When this is done, two critical concepts become apparent. First, a discrete reflected wave does not "arrive" at a particular moment after a forward wave is reflected from the periphery. In fact, since the pulse wave velocity is nearly 500 cm/s (63), reflected waves arrive continually as pulse waves are reflected and re-reflected several times in every heartbeat, which explains why a forward wave exists during diastole (11). In fact, there is no time when this composite reflected wave does not exist—in early systole, the wave is negative (Fig. A-8), rather than zero as is commonly assumed (49). This fundamental issue can explain why Segers et al. (96) reported that analysis of the pressure wave alone yielded inaccurate estimates of when the reflected wave "arrives". Second, reflected waves add both constructively and destructively with the forward wave at different times in the cardiac cycle (Fig. A-7B). In the case of the data from the 28 year old subject in Fig. A-8E, the reflected wave actually has a negative value at the time of peak systole. When the less appropriate method for wave separation analysis is applied, it can appears that the reflected wave can only "augment" systolic pressure, because it appears to have a very

large mean value. The present work is consistent with earlier reports that the reflected pulse wave can actually decrease pulse pressure (11, 86).

4.3.2 Implications of "Windkesselness" of an arterial system

The classical Windkessel model proposed by Otto Frank has an implicit assumption that pressures in the large arteries rise and fall simultaneously (77), which is equivalent to the assumption of infinite pulse wavelength (84). Although pulse wavelengths in humans are normally much longer than the arterial system, they can become even longer if heart rate decreases or if arteries become stiffer and pulse wave velocity increases (66). Three separate methods have been previously reported that indicate that an arterial system can degenerate into a classical Windkessel: 1) a Windkessel was analytically proven to be a first-order approximation of a simple distributed arterial system model using a Taylor Series approximation (84), 2) numerical evaluation of a realistic large-scale distributed arterial system model (like the one in the present work) was shown to act like a Windkessel when either heart rate or arterial compliance decreases (66), and 3) measured data in hypertensive animals were shown to be equivalent to pressures predicted from Windkessels with the same total arterial compliance and total peripheral resistance (83, 85). It has been recently estimated that a normal, young human aortic pressure pulse shows 95% correlation to that of a Windkessel. This correlation in aortic pressure pulse increases to 99% with age (66). Manifestation of "Windkesselness" in an arterial system leads to three important properties. First, the pulse wave length become very long, and therefore pulses get reflected and re-reflected many times between the heart and reflection sites (11), making

it inappropriate to describe reflection of a single wave returning from the periphery. Second, as pulse wavelength increases, the lengths of arteries cease to effect pulsatile pressure. Third, since total arterial compliance and total peripheral resistance are the only arterial parameters affecting pulsatile pressure, most of the physical parameters that investigators typically associate with pulse wave reflection—distances of reflection sites from the heart and the amount of local reflection generated locally—cease to be relevant (84). It is the degeneration of arterial system into a Windkessel that provides the greatest challenge to conventional interpretations of the Conventional Augmentation Index. In fact, we can now identify *Type D* pulse morphologies to be a manifestation of the degeneration of an arterial system into a Windkessel (Fig. A-11). In fact, the "True Augmentation Index" indicated no significant augmentation of pulse pressure in subjects over 50 years, i.e., when the system has already degenerated in to a classical Windkessel (Fig. A-9). However, to calculate TAI, it is required to measure pressure and flow simultaneously, as well as estimation of Z_o. This imposes difficulty in its clinical use which is further discussed in section 6.3.

4.3.3 Rearranging a spatially-distributed model to show evidence of Windkesselness

The large-scale human systemic arterial system model (129) was exploited in a new way in the present work to illustrate that the location of reflection sites and the amount of refection from bifurcations cease to be relevant to pulsatile pressure when the arterial system is stiff. With the goal of altering the location of reflection sites in an arterial system stiff enough to act like a Windkessel, the segments of limbs of the

Westerhof model were theoretically “amputated” and reattached to contralateral locations (Fig. A-10B). This re-arrangement made the network asymmetric, created new sites of reflection, and changed the distance of reflection sites from the heart. However, since input flow, total peripheral resistance, and total arterial compliance did not change with rearrangement, the predicted pressures were unaffected (compare Fig. A-10D with Fig. A-10E). This is result is particularly striking because there is typically very little reflection at any one bifurcation in an arterial system (52), which was previously verified for the Westerhof model (128). Because these results suggest that the elderly have Windkessel-like arterial systems, it becomes clear why there has been conflicting reports concerning changes to the distances to reflection sites with age (65). The process of determining an “effective length” (21, 72) not only is problematic because there is not enough information in measured pressure and flow to solve the hemodynamic inverse problem (21, 89), arterial length can become irrelevant. The insight that the location of reflection sites becomes unimportant when the system acts like a Windkessel may explain results of Taylor et al. (118), who determined the input impedance of a network of elastic tubes with randomly selected lengths. The fact that the resulting input impedances were similar to measured aortic input impedances (77) may have been illustrating “Windkesselness” of their system, and therefore the relative unimportance of spatial distribution. The approach of rearranging the classical Westerhof model is another example of a result that cannot come from experimental approaches, but from mathematical modeling based on fundamental principles.

5. INTERACTION OF AN AXIAL-FLOW LVAD AND THE CARDIOVASCULAR SYSTEM

Although animal models, mock circulations, and computational fluid dynamics provide necessary tools to characterize the interaction of an axial flow LVAD and the cardiovascular system, they are not sufficient; the many variables influencing the interaction either cannot be measured or controlled, and the generality of results are limited. The inability of computational, physical, or animal models to predict the behavior of LVAD-heart-arterial system interactions in humans impacts all phases of LVAD development. Investigators have thus begun reporting mathematical models that integrate the time-varying elastance model, an axial-flow LVAD, and a lumped arterial system (25, 68, 124). As of yet, none have addressed which combinations of cardiovascular parameters affect aortic valve opening, LVAD regurgitation, or ventricular collapse. More importantly, all solutions have been numerical. The results therefore pertain to the particular set of parameters used for the simulations, and entire studies would have to be duplicated to extend results to another mammal, patient population, or even physiological state. Furthermore, these relatively simple models have not been tested against more complex, realistic human models to discount the potential of pulse wave propagation and reflection to alter critical conclusions. In essence, conventional LVAD-heart-arterial system models may be too simple to trust, but too complex to be employed as a tool for clinical investigators.

In this section, Sunagawa's heart-arterial system model will be extended to develop an algebraic formula predicting ventricular-arterial-LVAD interaction in

mammals. The extended model will be tested against a realistic, large-scale human arterial system model proposed by Westerhof et al. (129).

5.1 Theory

5.1.1 Modeling the arterial system

Derived by Otto Frank more than a century ago, the classical (2-element) Windkessel model is a first-order approximation of the arterial system (92). Based on conservation of mass, the blood volume stored by the large arteries is equal to the difference of the volume of blood injected by the heart and the volume of blood leaving through the small resistance arteries. A simple differential equation was formed that related aortic pressure and flow to total arterial resistance (R_{tot}) and total arterial compliance (C_{tot}). In diastole, flow into the system ceases, and end-diastolic pressure (P_{ed}) can be expressed as a function of R_{tot}, C_{tot}, end-systolic pressure (P_{es}) and the diastolic period T_d.

$$P_{ed} = P_{es}.e^{\frac{-T_d}{R_{tot}C_{tot}}} \qquad (5.1)$$

In systole, the ventricle and arterial system are coupled. Sunagawa et al. (115) applied the principle of conservation of mass to relate three quantities. First, the volume injected into the arterial system is equal to the volume passing through the aortic valve (V_{valve}). Second, the volume stored in the aorta in systole is equal to C_{tot} multiplied by the change in aortic pressure (i.e., P_{es}-P_{ed}). Third, the volume leaving the arterial system is a

function of mean aortic pressure, R_{tot} and the systolic period (T_s). To simplify, mean arterial pressure was approximated by P_{es}.

$$V_{valve} = C_{tot}\left(P_{es} - P_{ed}\right) + \frac{P_{es}T_S}{R_{tot}} \tag{5.2}$$

In this case, V_{valve} is equal to stroke volume.

5.1.2 Time-varying elastance

The many disparate phenomena that effect cardiac function, including the Frank-Starling Effect (33, 104), the Bainbridge Effect (7), the Hill Effect (37) and the nonlinear end-diastolic pressure volume relationship (111), make cardiac output sensitive to both cardiac preload and afterload. To characterize the contractile properties of ventricles independent of the preload and afterload, Suga et al. developed the time-varying elastance concept (113, 114). Ventricular elastance (E) is expressed as a ratio of ventricular pressure (P_{LV}) to ventricular volume (V_{LV}), and is a function of time (t),

$$E(t) = \frac{P_{LV}(t)}{V_{LV}(t) - V_o} \tag{5.3}$$

where V_o is the dead volume (i.e., volume at zero pressure). Although it notably lacks behavior such as Hill Effect (37), this simple first-order empirical relationship, captures the Frank-Starling effect, where an increase in volume leads to an increase in pressure generated. Since E_{max} is the slope *of* the end-systolic pressure-volume relationship, it is often used as an index of ventricular contractility. E_{min}, the slope of the end-diastolic pressure-volume relationship, is used to characterize the diastolic function.

Since changes in ventricular contractility, diastolic function, and heart rate can be conveniently described by scaling E_{max}, E_{min}, and t, the time-varying elastance model has become a basis for numerous cardiovascular system models, especially those exploring heart-arterial interaction (10, 19, 98, 111).

5.1.3 Characterizing heart-arterial system interaction

Sunagawa et al. (115) integrated the first-order approximation of the left ventricle *Eq. 5.3* and the first-order description of the arterial system in diastole *Eq. 5.1* and systole *Eq. 5.2*. Their first important insight was that the full functional form of $E(t)$ was not necessary to estimate V_{valve}. In fact, V_{valve} can be calculated from the difference of end-diastolic volume (V_{ed}) and end-systolic volume (V_{es}). The dead volume (V_o) was neglected to simplify the derivation. From *Eq. 5.*3, the value of V_{es} is equal to V_{ed}-V_{valve}. Assuming that ventricular pressure at end diastole could be approximated by atrial pressure (P_{atria}), and that V_{ed} is equal to P_{atria}/E_{min}, *Eq. 5.*3 can be reformulated.

$$P_{es} = E_{max}V_{es} = E_{max}\left(\frac{P_{atria}}{E_{min}} - V_{valve}\right) \qquad (5.4)$$

Solving *Eq. 5.1-2* and *Eq. 5.*4 simultaneously, Sunagawa et al. (115) developed an algebraic formula for V_{valve} (which is equal to stroke volume) in terms of both heart and arterial system properties,

$$V_{valve} = \frac{E_{max} V_{ed}}{E_{max} + E_a} \tag{5.5}$$

where E_a is a constant related to arterial system parameters, as well systolic and diastolic periods,

$$E_a = \frac{R_{tot}}{T_S + (1 - e^{\frac{T_d}{R_{tot} C_{tot}}})} \tag{5.6}$$

Although E_a has been denoted the "effective arterial elastance" (115) because it is equal to the slope of the arterial system pressure-volume relationship, it is not directly related to arterial mechanical properties.

5.1.4 Modifying input into Windkessel

The classical (2-element) Windkessel described by *Eq. 5.1* and *5.2* assumed that the only injection of blood volume came directly from the heart through the aortic valve. However, an axial-flow LVAD continuously removes blood from the ventricle and injects it into the aorta in both systole and diastole and thus equal to mean LVAD flow (Q_{LVAD}). Modifying *Eq. 5.1* appropriately (by solving the differential equation with a steady input) yields a simple analytical solution.

$$P_{ed} = (P_{es} - Q_{LVAD}.R_{tot}).e^{\frac{-T_d}{R_{tot}.C_{tot}}} + Q_{LVAD}.R_{tot} \tag{5.7}$$

Similarly, *Eq. 5.2* describing heart-arterial system interaction in systole, can be modified to describe LVAD-heart-arterial system interaction. The volume injected into

the arterial system is equal to the volume is ejected through the aortic valves plus the volume injected by the LVAD, $Q_{LVAD} \cdot T_s$.

$$V_{valve} + Q_{LVAD} \cdot T_s = C_{tot}\left(P_{es} - P_{ed}\right) + \frac{P_{es}}{R_{tot}} T_s \qquad (5.8)$$

When the LVAD flow is set to zero, *Eq. 5.7* and *5.8* degenerate into the standard windkessel approximations *Eq. 5.2* and *5.3*.

5.1.5 Integrating ventricular and arterial system models in presence of axial-flow LVAD

Just as the equations describing flow into a Windkessel *Eq. 5.1* and *Eq. 5.2* were reformulated for the presence of an axial-flow LVAD *Eq. 5.7* and *Eq. 5.8*, equations describing flow out of a ventricle can be reformulated. Here, the value of V_{es} described in *Eq. 5.4* is decremented by the volume withdrawn by the LVAD during systole, $Q_{LVAD} \cdot T_s$.

$$P_{es} = E_{max} \cdot V_{es} = E_{max}\left(\frac{P_{atria}}{E_{min}} - V_{valve} - Q_{LVAD} \cdot T_s\right) \qquad (5.9)$$

When the LVAD flow is set to zero, *Eq. 5.9* degenerates into *Eq. 5.4*. Solving *Eq. 7-9* for V_{valve} yields an equation predicting the volume expelled through the aortic valves.

$$V_{valve} = \frac{E_{max} V_{ed}}{E_{max} + E_a} - \frac{R_{tot} + E_{max} T_s}{E_{max} + E_a} Q_{LVAD} \qquad (5.10)$$

The value of V_{valve} in *Eq. 5.10* represents the extension of the Sunagawa approximation for LVAD-heart-arterial system interaction. *Eq. 5.10* degenerates to original formulation of Sunagawa et al. (115) *Eq. 5.5* when Q_{LVAD} is set to zero.

5.1.6 Illustrative example application: persistent valve closure during systole

Eq. 5.10 provides a novel means to predict when LVAD flow is high enough to prevent ejection through the aortic valves. In this case, the aortic valves no longer open in systole, and all flow into the arterial system is due to the LVAD. This critical LVAD flow ($Q_{LVADmax}$) can be found by setting $V_{valve} = 0$ in *Eq. 5.10* and solving for Q_{LVAD}.

$$Q_{LVAD\max} = \frac{E_{\max}}{R_{tot} + E_{\max} T_s} \frac{P_{atria}}{E_{\min}} \tag{5.11}$$

This single exercise reveals the parameters that affect persistent valve closure: ventricular contractility, atrial pressure, total arterial resistance, diastolic function and systolic period.

5.1.7 Large-scale, realistic, human systemic arterial system model

The large-scale, realistic, human arterial system model developed by Westerhof et al. (129) was used as the recognized modeling "gold standard" (83, 99, 106) to test the validity of *Eq. 5.10*. Input into this model was a time-varying elastance model *Eq. 5.1* used to mimic the left ventricle. Atrial pressure (P_{atria}) was maintained at 5 mmHg. The particular time-varying elastance function used for simulation, was digitized from (114). The value of 1.5mmHg/ml for E_{max} was chosen to represent a normal healthy heart (94). To simulate varying degrees of heart failure, E_{max} was progressively decreased to 0.25 mmHg/ml. The steady-flow LVAD was modeled as constant flow source, and the LVAD outlet was placed in the ascending aorta. The model was implemented in Simulink (The Mathworks, Inc., 2005) and solved numerically, as described in detail elsewhere (66).

First, the large-scale model was used to predict pulsatile aortic pressure with different levels of Q_{LVAD}. Then this model was used to predict total aortic flow as a function of Q_{LVAD} and E_{max} and compared to the simple algebraic formula *Eq. 5.10*.

5.2 Results

Increasing flow of the axial-flow LVAD caused pulse pressure to decrease. Fig. A-12 illustrates the change in aortic pulse pressure with increasing mean LVAD flows predicted from the realistic, large-scale human arterial system model.

In general, as either LVAD flow or ventricular contractility increases, total flow into the aorta increases. Fig. A-13 illustrates how total flow into the aorta is affected by both LVAD flow and ventricular contractility (i.e., the value of E_{max}) predicted by the realistic, large-scale human arterial system model and from the simple algebraic formula given by *Eq. 5.10*. The deviation of simple algebraic formula from the realistic, large-scale human model was no more than 15% from that provided by the simple algebraic formula *Eq. 5.10*. For low values of E_{max}, total flow exhibits a plateau that is equal to LVAD flow. The plateau indicates the combinations of Q_{LVAD} and E_{max} that cause persistent aortic valve closure and thus shunting of all blood through the LVAD.

As the LVAD flow increases, more blood bypasses the aortic valve. Fig. A-14 illustrates how the percent of total flow into the aorta due to cardiac ejection changes as LVAD flow is increased. When E_{max} is 25% normal values, moderate increases in LVAD flow causes the aortic valve to close throughout the cardiac cycle.

Maximum LVAD flow found to be most sensitive to cardiac contractility and atrial pressure. Fig. A-15 illustrates how changing each of the critical arterial system properties determine the critical LVAD flow [$Q_{LVADmax}$, *Eq. 5.11*], the flow that causes the aortic valve to remain closed throughout the cardiac cycle. $Q_{LVADmax}$ flow can be increased with greater ventricular contractility (E_{max}), heart rate (HR) and atrial pressure (P_{atria}). On the other hand, as the systemic total arterial resistance (R_{tot}) increases, $Q_{LVADmax}$ decreases.

5.3 Discussion

This work developed a simple and accurate algebraic formula for aortic blood flow resulting from the complex interaction of the heart, arterial system and an axial-flow LVAD. Extending the theoretical framework of Sunagawa et al. (115) Characterizing heart-arterial system interaction, the present work provides critical insight into the relative contributions of the most important ventricular, arterial, and LVAD parameters effecting systemic perfusion and blood pressure. Since this approximation is based on the physics of blood flow, it can predict behavior. The approximation may therefore complement the conventional tools of computational fluid dynamics, mock circulations, or animal experimentations. In particular, the simple algebraic formula may provide insight into 1) patient selection, by suggesting when ventricular contractility is too low to open aortic valves, 2) design of LVAD controllers, by basing their algorithms on physiological principles, 3) development of performance and safety criteria, by scaling device test results from mammals to humans, and 4) optimizing devices for particular patient populations, e.g., designing LVADs for infants. The simple algebraic formula

was tested against a realistic, large-scale human cardiovascular system model, and was found to be accurate.

5.3.1 Accuracy of the simple algebraic formula

This work proposes a simple algebraic formula characterizing the complex interaction of the heart, systemic arterial system and LVAD. For simplicity, the arterial system is considered as classical (2-element) Windkessel model described by Frank (92). Though this simple model was criticized (3), it has been shown recently that the arterial system can be approximated by a Windkessel when arterial compliance is low, which is common among the population receiving LVADs (66). Although the arterial system model could have been described by 3-, 4- or 5-element models (34, 108, 130), only the classical (2-element) Windkessel has parameter values that are directly related to arterial system properties (92). Thus, we were able to test the approximation against the well-accepted large-scale distributed arterial system model developed by Westerhof et al. (129), and found it accurate to within 15% over a wide range of parameter values (Fig. A-13). This fairly high degree of agreement results primarily from the fact that a normal arterial system acts very much like a classical Windkessel. In fact, Mohiuddin et al. (66) found that the pulse pressure predicted from a Windkessel is 95% correlated to the pulse pressure calculated from the large-scale Westerhof model. Notably, the Windkessel approximation eliminates the dicrotic notch (66), which can explain why the greatest deviation in Fig. A-13 occurs at the critical points where aortic valve closure is affected. Interestingly, if LVAD flow is chosen to be zero, the approximation degenerates to Sunagawa's approximation (115) for heart-arterial system interaction. In fact, this may be

the first time that the Sunagawa approximation (i.e., Q_{LVAD} = 0, Fig. A-14) has been tested for accuracy against a modeling "gold standard" where all arterial properties are known. Such a test cannot be performed rigorously in animal models, since some parameters, e.g., E_{max}, cannot easily be measured in patients.

5.3.2 Balancing the elegance of a simple algebraic formula with the accuracy of a numerical solution

The present work provides the only known analytical (i.e., algebraic) approximation that predicts LVAD-heart-arterial system interaction. Although the simplifications embodied in *Eq. 5.10* may incur error in predicted flow, this cost must be balanced with the value of a predictive, algebraic formula. First, an analytical (i.e., algebraic) formulation allows critical insight. Not only are the most important parameters for determining LVAD performance identified *Eq. 5.10*, the interaction of parameters are explicit. Second, the equations can predict unintended consequences when the device is implanted. For instance, fibrosis from previous surgeries could make LVAD cannula placement in the thoracic aorta attractive. However, *Eq. 5.11* and Figs. A-13, A-14 and A-15 suggest that if ventricular contractility is particularly low, the aortic valve will cease to open during systole, resulting in higher probability of thrombosis in the aortic root. Third, *Eq. 5.10* may provide the basis for a physiology-based controller. Since this equation is predictive, it could be used to tune controller parameters for different patients, or even allow for predictive adaptive control (6, 36). Fourth, the predictive and intuitive nature of the simple algebraic formula may work synergistically to allow rational device design. Thus, this approximation may help limit inefficient trial-

and-error approaches in the design process. Fifth, the predictive nature of the equations may help predict how device performance may change in the critical transition from animal testing to human clinical trials.

5.3.3 The realistic, distributed arterial system model provides additional information

Although the realistic, large-scale human cardiovascular model may incrementally increase accuracy of predictions, its true strength lies in its ability to characterize behavior that is not captured by the Windkessel-based first order approximation *Eq. 5.10*: pulse wave propagation and reflection. The pulse pressure at different locations of the system is predicted by this realistic large-scale model. This model therefore may better predict behavior such as aortic valve opening. Also, this realistic model can be used to predict changes in LVAD performance when the outlet cannula is placed along different locations along the aorta or when particular arterial system parameters change.

6. SUMMARY AND INTEGRATION

6.1 Windkessel can be used as a predictive model

The use of the Windkessel in section 4 represents a major departure from convention. Typically, a version of the Windkessel model is used to solve the inverse problem. That is, parameters such as C_{tot} are unknown, and its value is carefully chosen to best fit the measured data. Here, the process is reversed. Instead of retrieving information from fitting the parameters of the 3-element Windkessel (130), 4-element Windkessel (109) or 5-element Windkessel (34) to data, information is retrieved by analyzing the *deviation* of the classical (2-element) Windkessel from measured data. In this study, total arterial compliance is first determined from low-frequency apparent compliance (83), and then taken to be the value of compliance in the Windkessel model. Determining C_{tot} in this way does not (forcibly) fit the model to measured pressure and flow. Instead, Windkessel pressure is predicted from input flow, C_{tot} and R_{tot} (Fig. A-2B). Therefore, there is a much greater deviation of the model from the data at intermediate and high frequencies. Thus, in the present study, the Windkessel is used as a *predictive* model, and deviations are used as a means of quantifying the similarity of an arterial system to a Windkessel.

6.2 Critical role of mathematical modeling and model-based analysis of empirical data

This dissertation work has developed two complimentary approaches to test the hypothesis that the systemic arterial system degenerates into a classical Windkessel when pulse wavelengths increase sufficiently. The first approach used a novel analytical technique to quantify the "Windkesselness" of an arterial system (Fig. A-2). The second approach used a realistic, large-scale human systemic arterial system model to quantify how changes in each parameter affect the degree of "Windkesselness" (Fig. A-5). Taken together, these two approaches led us to the conclusion that it is the pulse wavelength (independent of particular heart rate, compliances, or radii) that determines whether an arterial system behaves like a Windkessel (Fig. A-6).

These results could not be obtained by experimental means because it is not possible to *independently* change heart rate, compliances or radii of the large conductance arteries in an experimental model. For instance, unless peripheral resistance is significantly manipulated, altering heart rate affects mean pressure, and thus compliances and radii of the large conductance arteries (45, 106). Similarly, attempts to decrease aortic compliance by encasing the aorta in plaster (80) or banding it (39) do not mimic naturally-occurring diseases and can only be accomplished surgically. Furthermore, in section 4, the limbs of large-scale model were rearranged, theoretically mimicking "amputation". There is no safe method of altering aortic compliance or radius, let alone amputation of limbs in human subjects. Instead, the novel index of "Windkesselness" provides a simple, minimally-invasive means to characterize hemodynamic changes in an individual over time or relative differences in experimental groups. Requiring only

measured pulsatile pressure and flow (e.g., Fig. A-8), this index provides a much-needed tool to explore how the mechanical properties of the arterial system change with naturally-occurring diseases, and is amenable for use in a clinical setting.

Mathematical modeling and model-based analysis of empirical data have provided us the missing tools to reveal that ISH is a manifestation of an arterial system that has degenerated into a Windkessel, and thus arterial pressure in ISH is a function only of aortic flow, total peripheral resistance, and total arterial compliance. This methodology helped to illustrate that estimation of augmentation index due to reflection is meaningless.

6.3 Instrumentalist use of AI is appropriate for clinical use

Although the present work introduced a "True Augmentation Index" (*TAI*) that indicates the true effect of pulse wave reflection on pulse pressure, it is not our intention to suggest its use clinically. To calculate the *TAI*, it is necessary to measure both aortic pressure and flow with instruments with high frequency responses. In contrast, the Conventional Augmentation Index has major advantages that have caused it to grow in popularity. First, unlike wave separation analysis (*Eq. 4.3*), only measured pressure is necessary to calculate the Conventional Augmentation Index, making it feasible for use in clinical environments. Second, increases in the Conventional Augmentation Index have been correlated with age (43) and the progression of cardiovascular diseases (131). Because the present work has illustrated that the interpretation of the Conventional Augmentation Index is inappropriate, it would be perilous to rely on changes in it to suggest new clinical treatments (131). However, taking an "instrumentalist" approach to

the use of the Conventional Augmentation Index may not be unwarranted. That is, if the Conventional Augmentation Index is used as a mere indicator of a morphological change in the pressure with a particular clinical intervention, then it retains its usefulness. An important contribution of the present work may therefore be that we reinterpret the Augmentation Index.

6.4 Limitation of the large-scale distributed model

The large-scale model, however, has its own limitations. Arterial compliances were assumed constant, although they are known to be pressure-dependent (and thus nonlinear). Venous return and total fluid volume are important clinical indices which change with heart rate and LVAD flow, yet were not incorporated into the present version of the model. Also, no regulatory phenomena (e.g., baroreceptor modulation of peripheral resistance) were included. The choice has been made, because we were interested in the role of particular arterial system parameters such as total peripheral resistance or ventricular contractility on mean aortic flow, and regulatory phenomena merely adjust these parameters. If adding additional complexity to the simple model presented here *Eq. 5.10* would require numerical solution, the approximation would lose its usefulness. However, adding complexity to the large-scale human arterial system model, if based on sound empirical data and physics, could help make it an even more effective LVAD test-bed that incorporates principles of applied physiology early in the design process.

6.5 Calculating reflection when the system behaves like a Windkessel

After half a decade of its dominance in the arena of mathematical modeling, classical (2-element) Windkessel model of systemic arterial system was left aside by the investigators. It is well-established that pulse wave propagation and reflection effects in a Windkessel (0-D model) is impossible to model (77).

However, in a human systemic arterial system, pulses are reflected and re-reflected many times in a single cardiac cycle (11), making it impossible to identify a discrete set of reflection sites (89). In fact, the magnitude and phase of reflection becomes a function of C_{tot} and R_{tot} (84). Although the pressure pulses can be analyzed into forward and reflected waves, the composite reflection at the aortic root cannot be attributed to any particular arterial system property such as arterial system length, changes in reflection site or magnitude of local reflection (87, 89). The fact that arterial systems degenerate into Windkessels explains why it becomes much easier to estimate total arterial compliance in hypertension (83)—total arterial compliance is the dominant determinant of pulsatile pressure.

REFERENCES

1. **Akaike H**. A new look at the statistical model identification. *IEEE Trans Autom Control* 19: 7-16, 1974.
2. **Amir O, Bracey AW, Smart FW, Delgado RM, 3rd, Shah N, Kar B**. A successful anticoagulation protocol for the first HeartMate II implantation in the United States. *Tex Heart Inst J* 32: 399-401, 2005.
3. **Apéria A**. Hemodynamical studies. *Skand Arch Physiol* 83: 1-230, 1940.
4. **Arnett DK, Boland LL, Evans GW, Riley W, Barnes R, Tyroler HA, Heiss G**. Hypertension and arterial stiffness: the atherosclerosis risk in communities study. ARIC Investigators. *Am J Hypertens* 13: 317-323, 2000.
5. **Avolio AP**. Multi-branched model of the human arterial system. *Med Biol Eng Comput* 18: 709-718, 1980.
6. **Ayre PJ, Lovell NH**. Identifying physiologically significant pumping states in implantable rotary blood pumps using non-invasive system observers. *Conf Proc IEEE Eng Med Biol Soc* 1: 439-442, 2003.
7. **Bainbridge FA**. The influence of venous filling upon the rate of the heart. *J Physiol* 50: 65-84, 1915.
8. **Beltran A, McVeigh G, Morgan D, Glasser SP, Neutel JM, Weber M, Finkelstein SM, Cohn JN**. Arterial compliance abnormalities in isolated systolic hypertension. *Am J Hypertens* 14: 1007-1011, 2001.

9. **Berger DS, Li JK**. Concurrent compliance reduction and increased peripheral resistance in the manifestation of isolated systolic hypertension. *Am J Cardiol* 65: 67-71, 1990.

10. **Berger DS, Li JK**. Temporal relationship between left-ventricular and arterial system elastances. *IEEE Trans Biomed Eng* 39: 404-410, 1992.

11. **Berger DS, Li JK, Laskey WK, Noordergraaf A**. Repeated reflection of waves in the systemic arterial system. *Am J Physiol Heart Circ Physiol* 264: H269-H281, 1993.

12. **Berger DS, Li JK, Noordergraaf A**. Differential effects of wave reflections and peripheral resistance on aortic blood pressure: a model-based study. *Am J Physiol Heart Circ Physiol* 266: H1626-H1642, 1994.

13. **Berger DS, Quick CM**. Reduction of a complex arterial tree into a simple Windkessel. *Heart Vessels* 13: 45, 2000.

14. **Berger DS, Robinson KA, Shroff SG**. Wave propagation in coupled left ventricle-arterial system - Implications for aortic pressure. *Hypertension* 27: 1079-1089, 1996.

15. **Bertram CD**. Measurement for implantable rotary blood pumps. *Physiol Meas* 26: R99-R117, 2005.

16. **Brin KP, Yin FCP**. Effect of nitroprusside on wave reflections in patients with heart-failure. *Ann Biomed Eng* 12: 135-150, 1984.

17. **Burattini R, Di Salvia PO**. Development of systemic arterial mechanical properties from infancy to adulthood interpreted by four-element Windkessel models. *J Appl Physiol* 103: 66-79, 2007.

18. **Burattini R, Gnudi G**. Computer identification of models for the arterial tree input impedance: comparison between two new simple models and first experimental results. *Med Biol Eng Comp* 20: 134-144, 1982.

19. **Burkhoff D, Mirsky I, Suga H**. Assessment of systolic and diastolic ventricular properties via pressure-volume analysis: a guide for clinical, translational, and basic researchers. *Am J Physiol Heart Circ Physiol* 289: H501-H512, 2005.

20. **Cameron JD, McGrath BP, Dart AM**. Use of radial artery applanation tonometry and a generalized transfer function to determine aortic pressure augmentation in subjects with treated hypertension. *J Am Coll Cardio* 32: 1214-1220, 1998.

21. **Campbell KB, Lee LC, Frasch HF, Noordergraaf A**. Pulse reflection sites and effective length of the arterial system. *Am J Physiol Heart Circ Physiol* 256: H1684-H1689, 1989.

22. **Canty JM, Jr., Klocke FJ, Mates RE**. Pressure and tone dependence of coronary diastolic input impedance and capacitance. *Am J Physiol Heart Circ Physiol* 248: H700-H711, 1985.

23. **Castro MA, Putman CM, Cebral JR**. Patient-specific computational fluid dynamics modeling of anterior communicating artery aneurysms: a study of the sensitivity of intra-aneurysmal flow patterns to flow conditions in the carotid arteries. *Am J Neuroradiol* 27: 2061-2068, 2006.

24. **Cohen MA, Taylor JA**. Short-term cardiovascular oscillations in man: measuring and modeling the physiologies. *J Physiol* 542: 669-683, 2002.

25. **Conlon M, Russel D, Mussivand T**. Development of a mathematical model of the human circulatory system. *Ann Biomed Eng* 34: 14, 2006.

26. **Cooley JW, Tukey JW**. An algorithm for machine calculation of complex fourier series. *Math Comp* 19: 297-301, 1965.

27. **DeBakey ME, Noon GP, Teitel ER**. The rotary blood pump: lessons learned and future directions. *Artif Organs* 28: 865-868, 2004.

28. **Duprez DA, De Buyzere ML, Rietzschel ER, Taes Y, Clement DL, Morgan D, Cohn JN**. Inverse relationship between aldosterone and large artery compliance in chronically treated heart failure patients. *Eur Heart J* 19: 1371-1376, 1998.

29. **Fantin F, Mattocks A, Bulpitt CJ, Banya W, Rakumar C**. Is augmentation index a good measure of vascular stiffness in the elderly? *Age Ageing* 36: 43-48, 2007.

30. **Feldman CM, Silver MA, Sobieski MA, Slaughter MS**. Management of aortic insufficiency with continuous flow left ventricular assist devices: bioprosthetic valve replacement. *J Heart Lung Transplant* 25: 1410-1412, 2006.

31. **Fiedler VB**. Effects of pulsatile and non-pulsatile perfusion on the isolated canine heart. *Res Exp Med* 179: 183-198, 1981.

32. **Finkelstein SM, Cohn JN**. First- and third-order models for determining arterial compliance. *J Hypertens* 10: S11-S14, 1992.

33. **Frank O**. Frank O. Zur Dynamik des Herzmuskels. J Biol. 1895;32:370-447. Translation from German: Chapman CP, Wasserman EB. On the dynamics of cardiac muscle. *Am Heart J* 58: 467-478, 1959.

34. **Goldwyn R, Watt TB.** Arterial pressure pulse contour analysis via a mathematical model for the clinical quantification of human vascular properties. *IEEE Trans Biomed Eng* 14: 11-17, 1967.

35. **Hale JF, McDonald DA, Womersley JR**. Velocity profiles of oscillating arterial flow, with some calculations of viscous drag and the Reynolds number. *J Physiol* 128: 629-640, 1955.

36. **Hall AW, Soykan O, Harken AH**. Physiologic control of cardiac assist devices. *Artif Organs* 20: 271-275, 1996.

37. **Hill A**. The maximum work and mechanical efficiency of human muscles, and their most economical speed. *J Physiol* 56: 19-41, 1922.

38. **Hoshi H, Asama J, Shinshi T, Ohuchi K, Nakamura M, Mizuno T, Arai H, Shimokohbe A, Takatani S**. Disposable magnetically levitated centrifugal blood pump: design and in vitro performance. *Artif Organs* 29: 520-526, 2005.

39. **Ioannou CV, Stergiopulos N, Katsamouris AN, Startchik I, Kalangos A, Licker MJ, Westerhof N, Morel DR**. Hemodynamics induced after acute reduction of proximal thoracic aorta compliance. *Eur J Vasc Endovasc Surg* 26: 195, 2003.

40. **Karakash JJ**. *Transmission lines and filter networks*. New York: Macmillian, 1950.

41. **Karantonis DM, Lovell NH, Ayre PJ, Mason DG, Cloherty SL**. Identification and classification of physiologically significant pumping states in an implantable rotary blood pump. *Artif Organs* 30: 671-679, 2006.

42. **Kawahito S, Takano T, Nakata K, Maeda T, Nonaka K, Linneweber J, Schulte-Eistrup S, Sato T, Mikami M, Glueck J, Nose Y**. Analysis of the arterial blood pressure waveform during left ventricular nonpulsatile assistance in animal models. *Artif Organs* 24: 816-820, 2000.

43. **Kelly R, Hayward C, Avolio AP, Orourke M**. Noninvasive determination of age-related-changes in the human arterial pulse. *Circulation* 80: 1652-1659, 1989.

44. **Kerkhoffs W, Schumacher O, Meyns B, Verbeken E, Leunens V, Bollen H, Reul H**. Design, development, and first in vivo results of an implantable ventricular assist device, MicroVad. *Artif Organs* 28: 904-910, 2004.

45. **Langewouters GJ, Wesseling KH, Goedhard WJ**. The static elastic properties of 45 human thoracic and 20 abdominal aortas in vitro and the parameters of a new model. *J Biomech* 17: 425-435, 1984.

46. **Laskey WK, Kussmaul WG**. Arterial wave reflection in heart-failure. *Circulation* 75: 711-722, 1987.

47. **Latham RD, Westerhof N, Sipkema P, Rubal BJ, Reuderink P, Murgo JP**. Regional wave travel and reflections along the human aorta: a study with six simultaneous micromanometric pressures. *Circulation* 72: 1257-1269, 1985.

48. **Learoyd BM, Taylor MG**. Alterations with age in the viscoelastic properties of human arterial walls. *Circ Res* 18: 278-292, 1966.

49. **Li JK**. Time domain resolution of forward and reflected waves in the aorta. *IEEE Trans Biomed Eng* 33: 783-785, 1986.

50. **Li JK, Cui T, Drzewiecki GM**. A nonlinear model of the arterial system incorporating a pressure-dependent compliance. *IEEE Trans Biomed Eng* 37: 673-678, 1990.

51. **Li JK, Noordergraaf A**. Similar pressure pulse propagation and reflection characteristics in aortas of mammals. *Am J Physiol Regulatory Integrative Comp Physiol* 261: R519-R521, 1991.

52. **Li JK**. Pulse-wave reflections at the aorto-iliac junction. *Angiology* 36: 516-521, 1985.

53. **Liu Z, Brin KP, Yin FC**. Estimation of total arterial compliance: an improved method and evaluation of current methods. *Am J Physiol Heart Circ Physiol* 251: H588-H600, 1986.

54. **London GM, Blacher J, Pannier B, Guerin AP, Marchais SJ, Safar ME**. Arterial wave reflections and survival in end-stage renal failure. *Hypertension* 38: 434-438, 2001.

55. **Loree H**. The Heartmate III: design and in vivo studies of a maglev centrifugal left ventricular assist device. *Artif Organs* 25: 386-391, 2001.

56. **Lucas CL, Wilcox BR, Ha B, Henry GW**. Comparison of time domain algorithms for estimating aortic characteristic impedance in humans. *IEEE Trans Biomed Eng* 35: 62-68, 1988.

57. **Magner JJ, Royston D**. Heart failure. *Br J Anaesth* 93: 74-85, 2004.

58. **Maher TR, Butler KC, Poirier VL, Gernes DB**. HeartMate left ventricular assist devices: a multigeneration of implanted blood pumps. *Artif Organs* 25: 422-426, 2001.

59. **McVeigh GE, Burns DE, Finkelstein SM, McDonald KM, Mock JE, Feske W, Carlyle PF, Flack J, Grimm R, Cohn JN**. Reduced vascular compliance as a marker for essential hypertension. *Am J Hypertens* 4: 245-251, 1991.

60. **Mielniczuk L, Mussivand T, Davies R, Mesana TG, Masters RG, Hendry PJ, Keon WJ, Haddad HA**. Patient selection for left ventricular assist devices. *Artif Organs* 28: 152-157, 2004.

61. **Mihaylov D, Verkerke GJ, Blanksma PK, Elstrodt J, De Jong ED, Rakhorst G**. Evaluation of the optimal driving mode during left ventricular assist with pulsatile catheter pump in calves. *Artif Organs* 23: 1117-1122, 1999.

62. **Miller LW, Lietz K**. Candidate selection for long-term left ventricular assist device therapy for refractory heart failure. *J Heart Lung Transplant* 25: 756-764, 2006.

63. **Milnor WR**. *Hemodynamics*. Baltimore, MD: Williams and Wilkins, 1989.

64. **Mitamura Y, Murabayashi S**. The Japanese artificial organs scene: current status. *Artif Organs* 29: 675-680, 2005.

65. **Mitchell GF, Parise H, Benjamin EJ, Larson MG, Keyes MJ, Vita JA, Vasan RS, Levy D**. Changes in arterial stiffness and wave reflection with advancing age in healthy men and women - The Framingham Heart Study. *Hypertension* 43: 1239-1245, 2004.

66. **Mohiuddin MW, Laine GA, Quick CM**. Increase in pulse wavelength causes the systemic arterial tree to degenerate into a classical Windkessel. *Am J Physiol Heart Circ Physiol* 293: H1164-H1171, 2007.

67. **Molino P, Cerutti C, Julien C, Cuisinaud G, Gustin M-P, Paultre C**. Beat-to-beat estimation of Windkessel model parameters in conscious rats. *Am J Physiol Heart Circ Physiol* 274: H171-H177, 1998.

68. **Morley D, Litwak K, Ferber P, Spence P, Dowling R, Meyns B, Griffith B, Burkhoff D**. Hemodynamic effects of partial ventricular support in chronic heart failure: results of simulation validated with in vivo data. *J Thorac Cardiovasc Surg* 133: 21-28, 2007.

69. **Murgo JP, Westerhof N, Giolma JP, Altobelli SA**. Aortic input impedance in normal man: relationship to pressure wave forms. *Circulation* 62: 105-116, 1980.

70. **Naka KK, Tweddel AC, Parthimos D, Henderson A, Goodfellow J, Frenneaux MP**. Arterial distensibility: acute changes following dynamic exercise in normal subjects. *Am J Physiol Heart Circ Physiol* 284: H970-H978, 2003.

71. **Nichols WW, Avolio AP, Kelly RP**. Effects of age and of hypertension on wave travel and reflection. In: *Arterial Vesodilation: mechanism and therapy*, edited by O'Rourke M, Safar, M,and Dzau, V. London: Edward Arnold, 23-40, 1993.

72. **Nichols WW, O'Rourke MF**. *McDonald's blood flow in arteries: theoretical, experimental, and clinical principles*. Philadelphia, PA: Arnold, 1998.

73. **Nichols WW, Edwards DG**. Arterial elastance and wave reflection augmentation of systolic blood pressure: deleterious effects and implications for therapy. *J Cardiovasc Pharmacol Ther* 6: 5-21, 2001.

74. **Nichols WW, Nicolini FA, Pepine CJ**. Determinants of isolated systolic hypertension in the elderly. *J Hypertens Suppl* 10: S73-S77, 1992.

75. **Nichols WW, O'Rourke MF, Avolio AP, Yaginuma T, Murgo JP, Pepine CJ, Conti CR**. Effects of age on ventricular-vascular coupling. *Am J Cardiol* 55: 1179-1184, 1985.

76. **Noon GP, Morley DL, Irwin S, Abdelsayed SV, Benkowski RJ, Lynch BE**. Clinical experience with the MicroMed DeBakey ventricular assist device. *Ann Thorac Surg* 71: S133-S138, 2001.

77. **Noordergraaf A**. *Circulatory system dynamics*. New York, NY: Academic Press, 1978.

78. **Noordergraaf A**. *Physical basis of ballistocordiography*. (PhD Dissertation) Utrecht, The Netherlands: University of Utrecht, 1956.

79. **O'Rourke MF**. Pressure and flow waves in systemic arteries and the anatomical design of the arterial system. *J Appl Physiol* 23: 139-149, 1967.

80. **O'Rourke MF**. Steady and pulsatile energy losses in the systemic circulation under normal conditions and in simulated disease. *Cardiovasc Res* 1: 313-326, 1967.

81. **O'Rourke MF, Kelly RP**. Wave reflection in the systemic circulation and its implications in ventricular function. *J Hypertens* 11: 327-337, 1993.

82. **Ohuchi K, Takatani S**. Currently available ventricular-assist devices: capabilities, limitations and future perspectives. *Expert Rev Med Devices* 3: 195-205, 2006.

83. **Quick CM, Berger DS, Hettrick DA, Noordergraaf A**. True arterial system compliance estimated from apparent arterial compliance. *Ann Biomed Eng* 28: 291-301, 2000.

84. **Quick CM, Berger DS, Noordergraaf A**. Apparent arterial compliance. *Am J Physiol Heart Circ Physiol* 274: H1393-H1403, 1998.

85. **Quick CM, Berger DS, Noordergraaf A**. Arterial pulse wave reflection as feedback. *IEEE Trans Biomed Eng* 49: 440-445, 2002.

86. **Quick CM, Berger DS, Noordergraaf A**. Constructive and destructive addition of forward and reflected arterial pulse waves. *Am J Physiol Heart Circ Physiol* 280: H1519-H1527, 2001.

87. **Quick CM, Berger DS, Stewart RH, Laine GA, Hartley CJ, Noordergraaf A**. Resolving the hemodynamic inverse problem. *IEEE Trans Biomed Eng* 53: 361-368, 2006.

88. **Quick CM, Mohiuddin MW, Laine GA, Noordergraaf A**. The arterial system pressure-volume loop. *Physiol Meas* 26: N29-N35, 2005.

89. **Quick CM, Young WL, Noordergraaf A**. Infinite number of solutions to the hemodynamic inverse problem. *Am J Physiol Heart Circ Physiol* 280: H1472-H1479, 2001.

90. **Randall OS, Esler MD, Calfee RV, Bulloch GF, Maisel AS, Culp B**. Arterial compliance in hypertension. *Aust NZ J Med* 6: 49-59, 1976.

91. **Remington JW**. *The physiology of the aorta and major arteries*. Washington, DC: American Physiology Society, 1963.

92. **Sagawa K, Lie RK, Schaefer J**. Translation of Otto Frank's paper "Die Grundform des Arteriellen Pulses" Zeitschrift fur Biologie 37: 483-526 (1899). *J Mol Cell Cardiol* 22: 253-277, 1990.

93. **Saito A, Shiono M, Orime Y, Yagi S, Nakata KI, Eda K, Hattori T, Funahashi M, Taniguchi Y, Negishi N, Sezai Y**. Effects of left ventricular assist device on cardiac function: experimental study of relationship between pump flow and left ventricular diastolic function. *Artif Organs* 25: 728-732, 2001.

94. **Segers P, Stergiopulos N, Schreuder JJ, Westerhof BE, Westerhof N**. Left ventricular wall stress normalization in chronic pressure-overloaded heart: a mathematical model study. *Am J Physiol Heart Circ Physiol* 279: H1120-H1127, 2000.

95. **Segers P, De Backer J, Devos D, Rabben SI, Gillebert TC, Van Bortel LM, De Sutter J, De Paepe A, Verdonck PR**. Aortic reflection coefficients and their association with global indexes of wave reflection in healthy controls and patients with Marfan's syndrome. *Am J Physiol Heart Circ Physiol* 290: H2385-H2392, 2006.

96. **Segers P, Rietzschel ER, De Buyzere ML, De Bacquer D, Van Bortel LM, De Backer G, Gillebert TC, Verdonck PR**. Assessment of pressure wave reflection: getting the timing right! *Physio Meas* 28: 1045-1056, 2007.

97. **Segers P, Rietzschel ER, De Buyzere ML, Vermeersch SJ, De Bacquer D, Van Bortel LM, De Backer G, Gillebert TC, Verdonck PR**. Noninvasive (input) impedance, pulse wave velocity, and wave reflection in healthy middle-aged men and women. *Hypertension* 49: 1248-1255, 2007.

98. **Segers P, Stergiopulos N, Westerhof B, Westerhof N**. Left ventricular wall stress normalization in chronic pressure-overloaded heart: a mathematical model study. *Am J Physiol Heart Circ Physiol* 279: H1120-H1127, 2000.

99. **Segers P, Stergiopulos N, Verdonck P, Verhoeven R**. Assessment of distributed arterial network models. *Med Biol Eng Comput* 35: 729-736, 1997.

100. **Segers P, Verdonck P**. Role of tapering in aortic wave reflection: hydraulic and mathematical model study. *J Biomech* 33: 299-306, 2000.

101. **Sharp MK, Pantalos GM, Minich L, Tani LY, McGough EC, Hawkins JA**. Aortic input impedance in infants and children. *J Appl Physiol* 88: 2227-2239, 2000.

102. **Shi Y, Korakianitis T**. Numerical simulation of cardiovascular dynamics with left heart failure and in-series pulsatile ventricular assist device. *Artif Organs* 30: 929-948, 2006.

103. **Siegenthaler MP, Westaby S, Frazier OH, Martin J, Banning A, Robson D, Pepper J, Poole-Wilson P, Beyersdorf F**. Advanced heart failure: feasibility study of long-term continuous axial flow pump support. *Eur Heart J* 26: 1031-1038, 2005.

104. **Starling EH**. *Linacre lecture on the law of the heart*. London: Longmans & Gree, 1918.

105. **Stergiopulos N, Meister JJ, Westerhof N**. Determinants of stroke volume and systolic and diastolic aortic pressure. *Am J Physiol Heart Circ Physiol* 270: H2050-H2059, 1996.

106. **Stergiopulos N, Meister JJ, Westerhof N**. Evaluation of methods for estimation of total arterial compliance. *Am J Physiol Heart Circ Physiol* 37: H1540-H1548, 1995.

107. **Stergiopulos N, Westerhof BE, Westerhof N**. Physical basis of pressure transfer from periphery to aorta: a model-based study. *Am J Physiol Heart Circ Physiol* 43: H1386-H1392, 1998.

108. **Stergiopulos N, Westerhof BE, Westerhof N**. Total arterial inertance as the fourth element of the Windkessel model. *Am J Physiol Heart Circ Physiol* 276: H81-H88, 1999.

109. **Stergiopulos N, Westerhof BE, Westerhof N**. Total arterial inertance as the fourth element of the Windkessel model. *Am J Physiol Heart Circ Physiol* 276: H81-H88, 1999.

110. **Stergiopulos N, Westerhof N**. Determinants of pulse pressure. *Hypertension* 32: 556-559, 1998.

111. **Suga H, Igarashi Y, Yamada O, Goto Y**. Mechanical efficiency of the left ventricle as a function of preload, afterload, and contractility. *Heart Vessels* 1: 3-8, 1985.

112. **Suga H, K. Sagawa, L. Demer**. Determinants of instantaneous pressure in canine left ventricle. Time and volume specification. *Circ Res* 46: 256-263, 1980.

113. **Suga H, Sagawa K**. Instantaneous pressure-volume relationships and their ratio in the excised, supported canine left ventricle. *Circ Res* 35: 117-126, 1974.

114. **Suga H, Sagawa K**. Mathematical interrelationship between instantaneous ventricular pressure-volume ratio and myocardial force-velocity relation. *Ann Biomed Eng* 1: 160-181, 1972.

115. **Sunagawa K, Sagawa K, Maughan WL**. Ventricular interaction with the loading system. *Ann Biomed Eng* 12: 163-189, 1984.

116. **Takazawa K**. Augmentation index in heart disease. *Am J Hyperten* 18: 15-18, 2005.

117. **Taylor MG**. An approach to an analysis of the arterial pulse wave. I. Oscillations in an attenuating line. *Phys Med Biol* 1: 258-269, 1957.

118. **Taylor MG**. The input impedance of an assembly of randomly branching elastic tubes. *Biophys J* 6: 29-51, 1966.

119. **Taylor MG**. Use of random excitation and spectral analysis in the study of frequency-dependent parameters of the cardiovascular system. *Circ Res* 18: 585-595, 1966.

120. **Taylor MG**. Wave travel in a non-uniform transmission line, in relation to pulses in arteries. *Phys Med Biol* 10: 539-550, 1965.

121. **Thalmann M, Schima H, Wieselthaler G, Wolner E**. Physiology of continuous blood flow in recipients of rotary cardiac assist devices. *J Heart Lung Transplant* 24: 237-245, 2005.

122. **Timms D, Hayne M, McNeil K, Galbraith A**. A complete mock circulation loop for the evaluation of left, right, and biventricular assist devices. *Artif Organs* 29: 564-572, 2005.

123. **Travis AR, Giridharan GA, Pantalos GM, Dowling RD, Prabhu SD, Slaughter MS, Sobieski M, Undar A, Farrar DJ, Koenig SC**. Vascular pulsatility in patients with a pulsatile- or continuous-flow ventricular assist device. *J Thorac Cardiovasc Surg* 133: 517-524, 2007.

124. **Vandenberghe S, Segers P, Meyns B, Verdonck P**. Unloading effect of a rotary blood pump assessed by mathematical modeling. *Artif Organs* 27: 1094-1101, 2003.

125. **Vandenberghe S, Segers P, Meyns B, Verdonck PR**. Effect of rotary blood pump failure on left ventricular energetics assessed by mathematical modeling. *Artif Organs* 26: 1032-1039, 2002.

126. **Vollkron M, Schima H, Huber L, Wieselthaler G**. Interaction of the cardiovascular system with an implanted rotary assist device: simulation study with a refined computer model. *Artif Organs* 26: 349-359, 2002.

127. **Welkowitz W, Fich S**. A nonuniform hybrid model of the aorta. *Trans N Y Acad Sci* 29: 316-331, 1967.

128. **Westerhof N**. *Analog studies of the human systemic arterial hemodynamics*. (PhD Dissertation) Philadelphia, PA: University of Pennsylvania, 1968.

129. **Westerhof N, Bosman F, De Vries CJ, Noordergraaf A**. Analog studies of the human systemic arterial tree. *J Biomech* 2: 121-143, 1969.

130. **Westerhof N, Elzinga G, Sipkema P**. An artificial arterial system for pumping hearts. *J Appl Physiol* 31: 776-781, 1971.

131. **Westerhof N, O'Rourke MF**. Haemodynamic basis for the development of left ventricular failure in systolic hypertension and for its logical therapy. *J Hypertens* 13: 943-952, 1995.

132. **Westerhof N, Sipkema P, van den Bos GC, Elzinga G**. Forward and backward waves in the arterial system. *Cardiovasc Res* 6: 648-656, 1972.

133. **Wetterer E**. Die Wirkung Der Herztatigkeit Auf Die Dynamik Des Arteriensystems. *Klinische Wochenschrift* 34: 609-609, 1956.

134. **Witzig K**. *Uber erzwungene Wellenbewegungen zaher, inkompressibler Flussigkeiten in elastischen Rohren*. (PhD Dissertation) Bern, Switzerland: University of Bern, 1914.

135. **Womersley JR**. Method for the calculation of velocity, rate of flow and viscous drag in arteries when the pressure gradient is known. *J Physiol* 127: 553-563, 1955.

136. **Womersley JR**. Oscillatory flow in arteries: the constrained elastic tube as a model of arterial flow and pulse transmission. *Phys Med Biol* 2: 178-187, 1957.

137. **Yano TS, Mitoh AK, Mitamura Y, Okamoto E, Kim DW, Nishimura I, Murabayashi S, Yozu R**. An estimation method of hemolysis within an axial flow blood pump by computational fluid dynamics analysis. *Artif Organs* 27: 26, 2003.

138. **Yin FC, Ting CT**. Compliance changes in physiological and pathological states. *J Hypertens Suppl* 10: S31-S33, 1992.

APPENDIX A

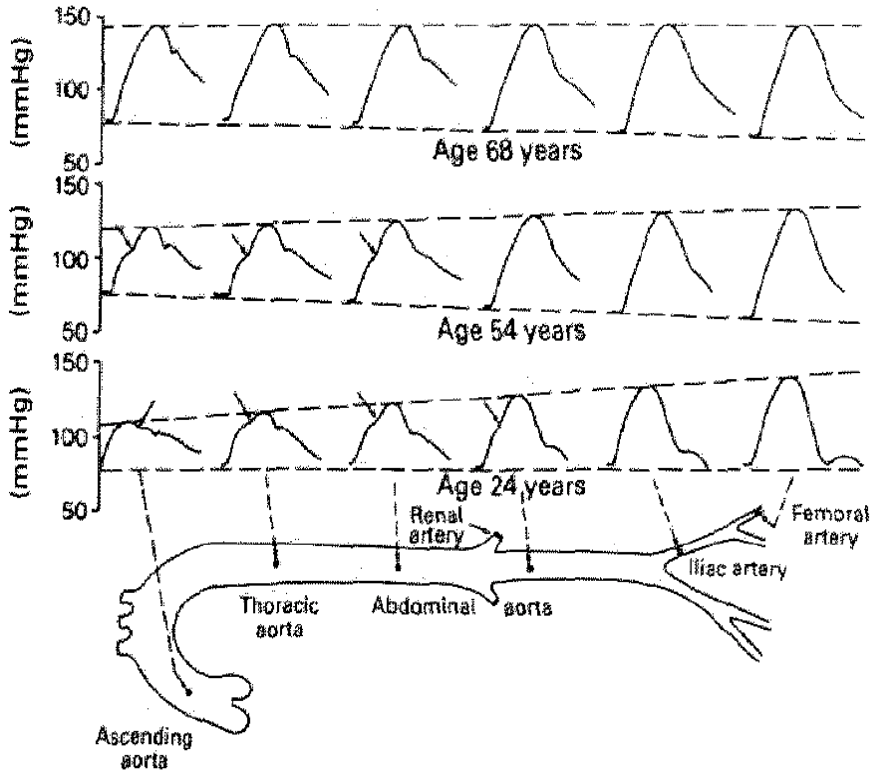

Figure A-1: Pressure waves recorded along the arterial tree from the proximal ascending aorta to the femoral artery in three human aged 28, 52 and 68 years. In the older subject, there is little amplification in the pressure wave during transmission, however, in the youngest subject, the amplitude of the pressure wave increases approximately 60% during transmission (71).

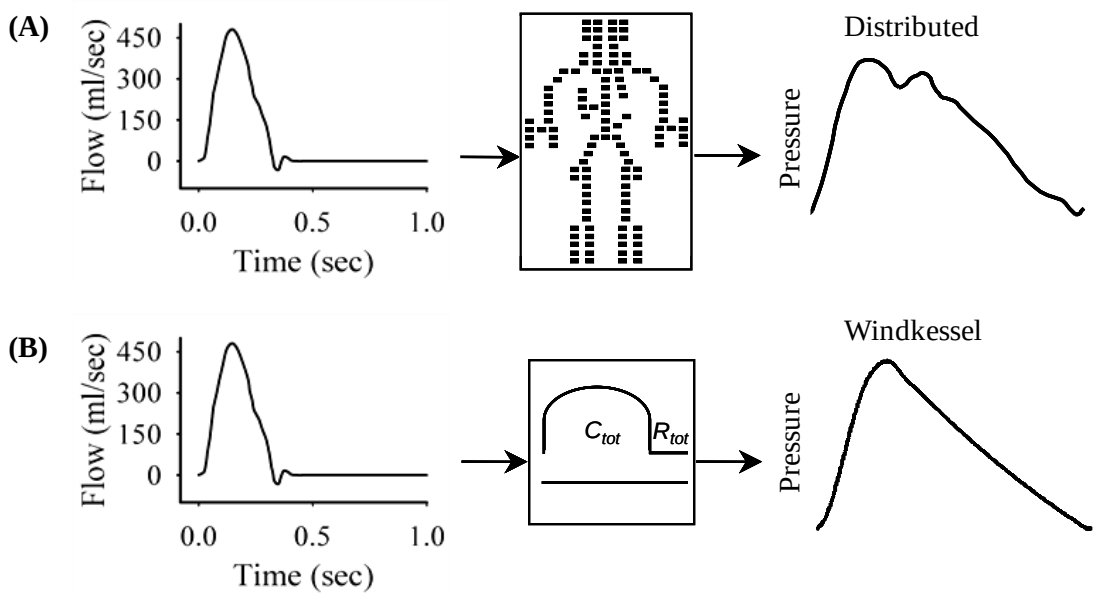

Figure A-2: Graphical representation of a method to determine the degree of "Windkesselness" of an arterial system. Input aortic flow was retrieved from digitizing experimentally determined flow in Fig. 1 from (106). Note that flow is not precisely zero in early diastole. (A) Graphical representation of a realistic human arterial system model originally described by Westerhof et al. (129). The 121 elements represent vessel segments. Predicted pressure (Distributed) includes effects of pulse wave propagation and reflection. (B) Graphical representation of a classical Windkessel model of the human arterial system originally described by Frank (92). Storage of blood is represented by a single chamber with compliance equal to total arterial compliance (C_{tot}), and resistance to blood flow is represented by a single outlet vessel with resistance equal to total peripheral resistance (R_{tot}). Predicted pressure (Windkessel) represents the pressure if the system had the same input flow, R_{tot} and C_{tot}, but behaved like a Windkessel. Correlation of Distributed and Windkessel pressures indicates the degree of "Windkesselness" in an arterial system.

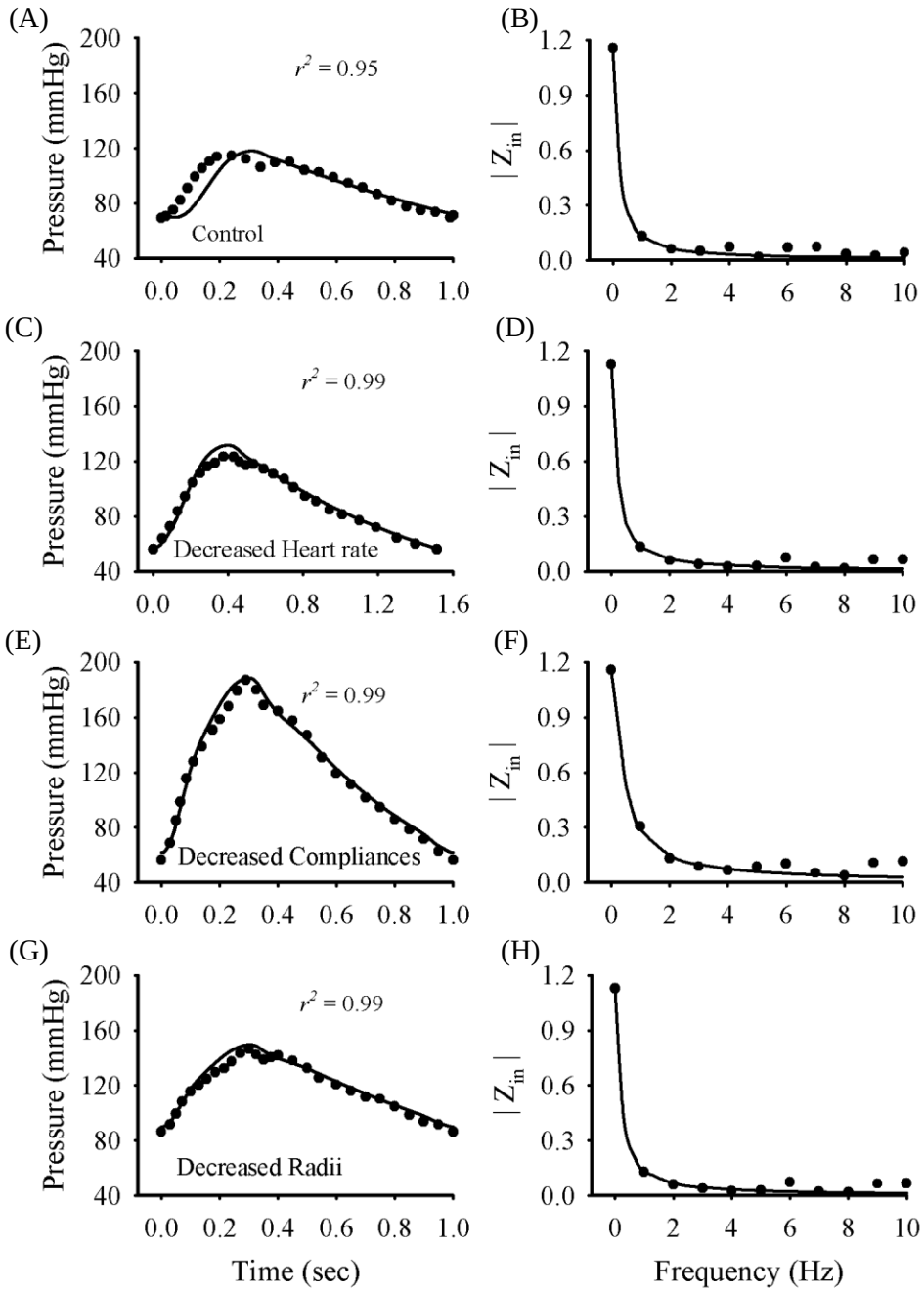

Figure A-3: Pressure and input impedances of the distributed human arterial system model (●) and the Windkessel model (solid line) when pulse wavelengths are made to increase 50% above normal (*Eq. 3.5*). (A&B) Normal values of arterial compliances, vessel radii, and heart rate. (C&D) Low heart rate (33.3% decrease), (E&F) Low compliance (55.5% decrease), and (G&H) Large vessel radii (50% increase). Similarity between distributed and Windkessel models indicates degeneration of system into a Windkessel when heart rate and compliances decrease, or vessel radii increase.

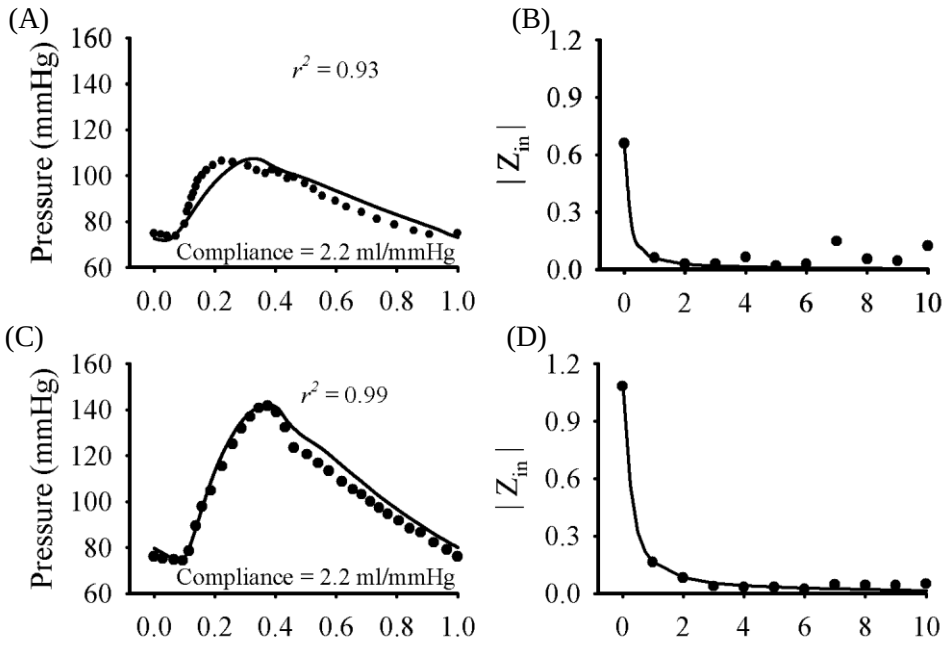

Figure A-4: Analysis of previously reported human data reveals that an arterial system can degenerate into a Windkessel with age. Measured aortic pressures and input impedances of human subjects compared to Windkessel predictions assuming the same total compliance and peripheral resistance. (A&B) Measured aortic pressure and input impedance of a 28 year old normotensive person (●) and corresponding Windkessel model prediction (line). (C&D) Measured aortic pressure and input impedance of a 68 year old person (●) and corresponding Windkessel prediction (line). Measured pressures and input impedances reproduced from Nichols et al. (71).

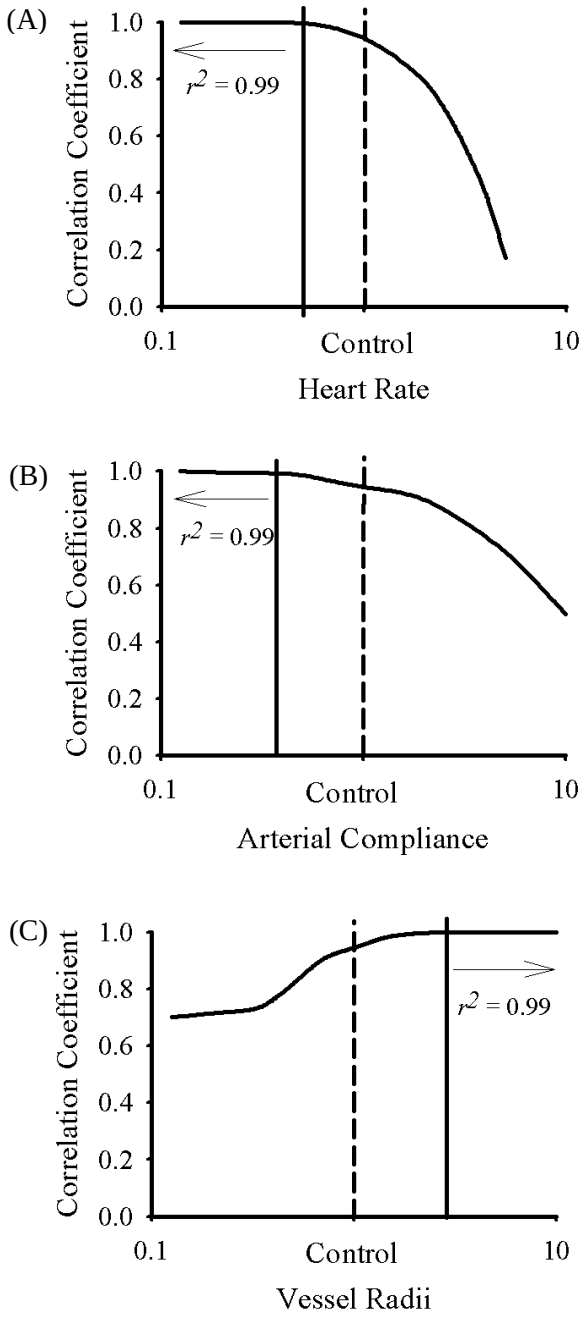

Figure A-5: Illustration of the degeneration of the human systemic arterial system model into a Windkessel indicated by increasing correlation between pressures predicted from large scale arterial system model and the Windkessel model. The distributed human systemic arterial system model degenerates into a Windkessel when heart rate decreases, arterial compliances decrease, and vessel radii increase. Heart rate, compliances, and radii expressed as factors of normal "control" values (indicated by dashed line).

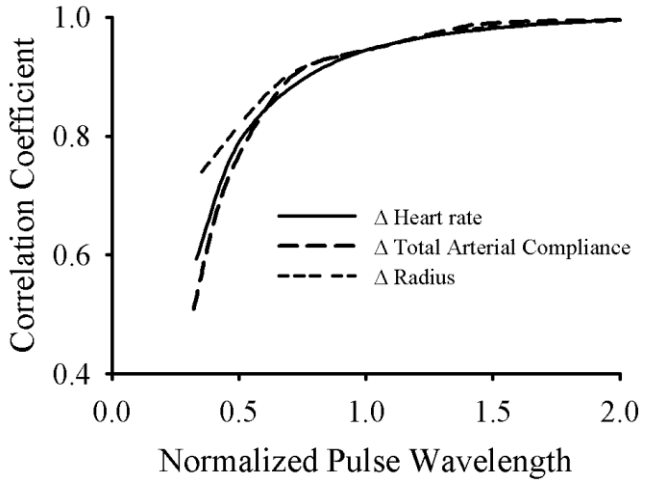

Figure A-6: Human arterial system degenerates into a Windkessel when pulse wavelength increases. Degeneration indicated by increase in correlation between pressures predicted from the large scale arterial system model and from the Windkessel. Although changes in heart rate, compliances, and vessel radii have disparate impact on "Windkesselness" of an arterial system (Fig. A-5), the resulting pulse wavelength vs. correlation coefficient relationships are very similar.

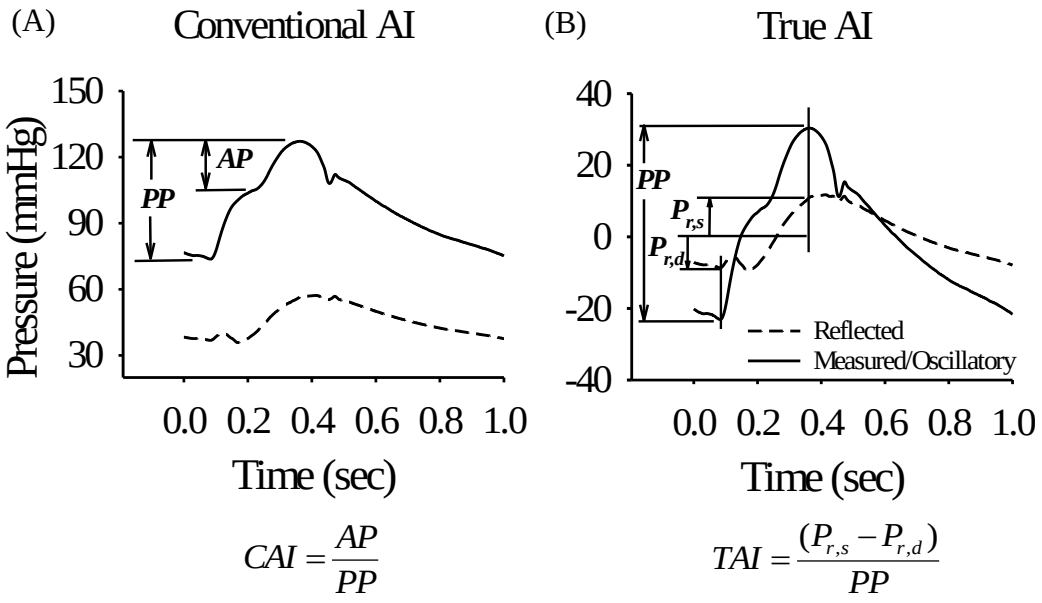

Figure A-7: (A) Illustration of the method to estimate the Conventional Augmentation Index (*CAI*). *AP* is the difference in pressure from an inflection point in the pressure wave to peak systolic pressure. The *CAI* is the ratio of the *AP* to the pulse pressure, *PP*. (B) Illustration of the proposed method to calculate true augmentation of pulse pressure by the reflected wave. Pressures at peak systole and end-diastole are augmented by the values of the reflected wave P_r at the time of peak systole ($P_{r,s}$) and end-diastole ($P_{r,d}$). The True Augmentation Index (*TAI*) is the ratio of ($P_{r,s}$-$P_{r,d}$) and *PP*. Pressure morphology was digitized from data originally reported in (71) and derives from a 52 years old normotensive subject.

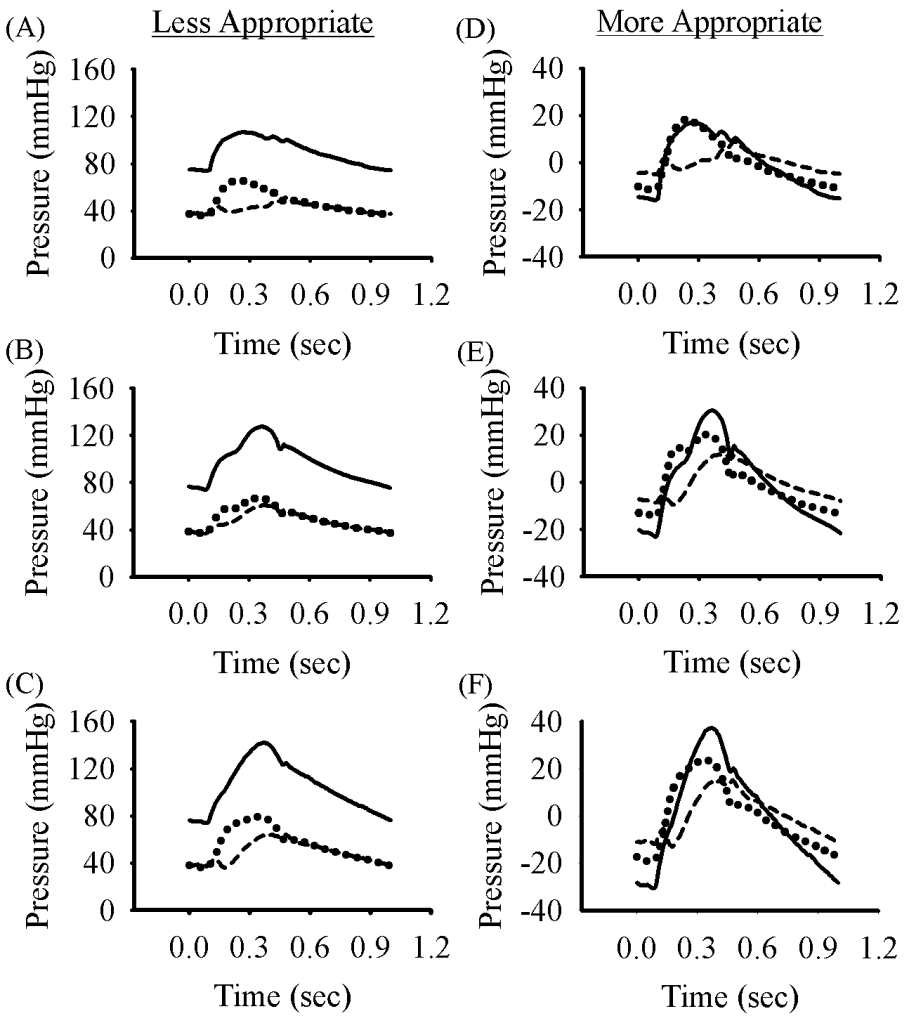

Figure A-8: Illustration of less and more appropriate application of wave separation analysis applied to data originally reported in Nichols et al. (71) from subjects of three different ages. (A-C) Estimation of forward and reflected pressure pulse waves using less appropriate application of wave separation analysis (*Eq. 4.2*) suggests that the reflected pulse always has positive values and therefore must augment peak systolic pressure. (C-E) Estimation of forward and reflected pressure pulse waves using more appropriate method (*Eq. 4.3*). More appropriate method indicates that the composite reflected pressure pulse wave does not necessarily augment systolic pressure, particularly for the youngest case.

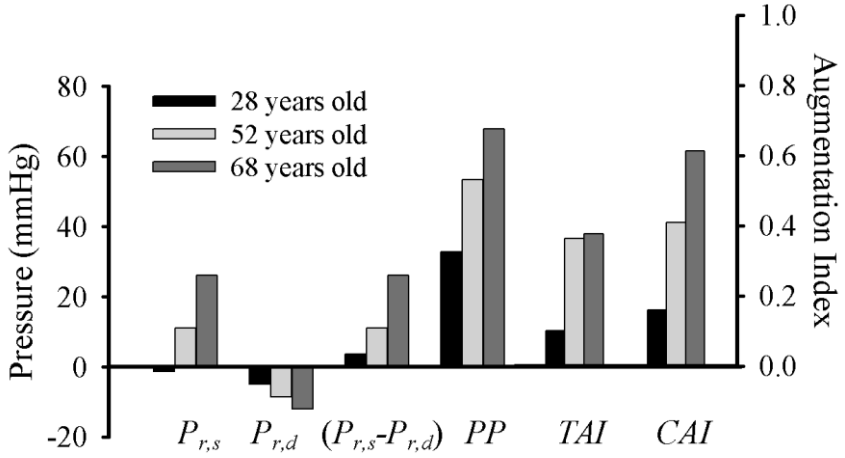

Figure A-9: Analysis of the data presented in Fig. A-8. Contribution of the composite reflected wave to peak systolic pressure (P_s), end-diastolic pressure (P_d), the contribution or the reflected pressure wave (P_r) to pulse pressure by raising P_s or lowering P_d ($P_{r,s}$-$P_{r,d}$), and the effect of the reflected pressure wave to the True Augmentation Index (*TAI*, *Eq. 4.5*) and the Conventional Augmentation Index (*CAI*, *Eq. 4.4*). Note that peak systolic pressure is lowered by reflection.

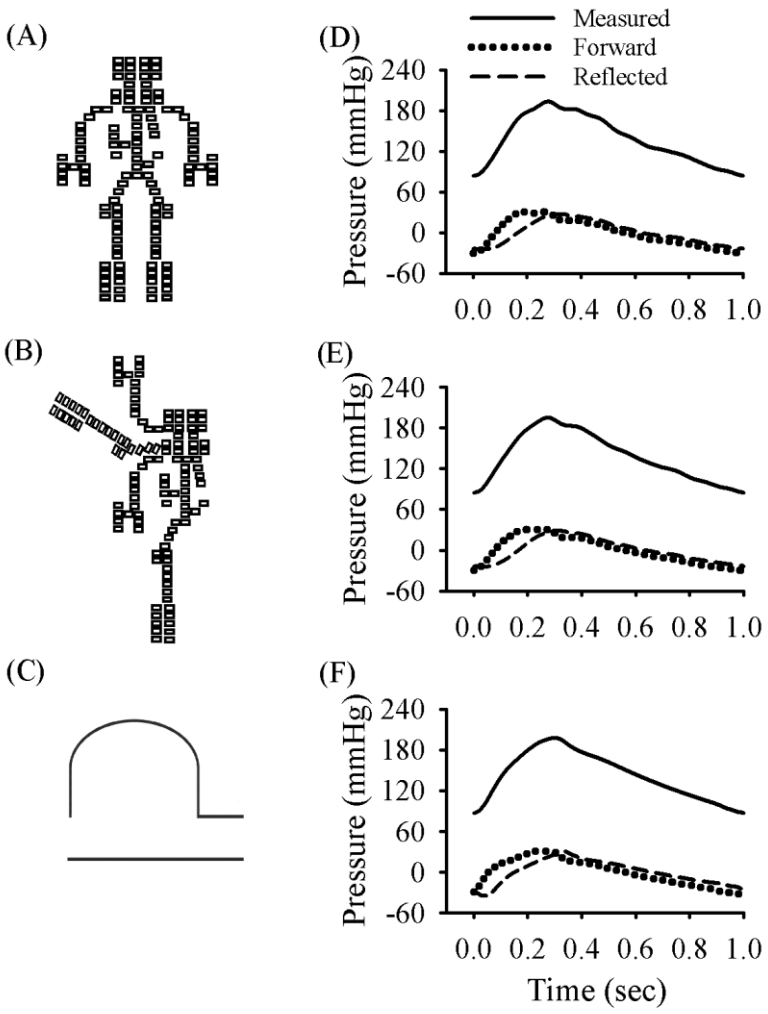

Figure A-10: Graphical representation of (A) realistic large-scale spatially-distributed model proposed by Westerhof et al. (132), (B) the same distributed model after rearrangement to create new reflection sites, and (C) a classical (2-element) Windkessel equivalent (see Fig. A-2B) which eliminates the influence of vessel length. Each model has the total arterial compliance of a 68 year old normotensive subject described elsewhere (74). (D) Pressure falls exponentially as is predicted for classical Windkessel. (E) Adding new reflection sites and changing distances to reflection sites result in similar pressures and forward and reflected waves as in A. (F) Pressure of the Windkessel equivalent is similar to pressures in distributed system (A and B), indicating the system in (A) is stiff enough to degenerate into a classical Windkessel. Composite forward and

reflected waves are almost identical in all three cases. Sites of reflection have no influence on aortic pressure and timing of reflected waves; total arterial compliance and total peripheral resistance are the most influential parameters governing pulse pressures.

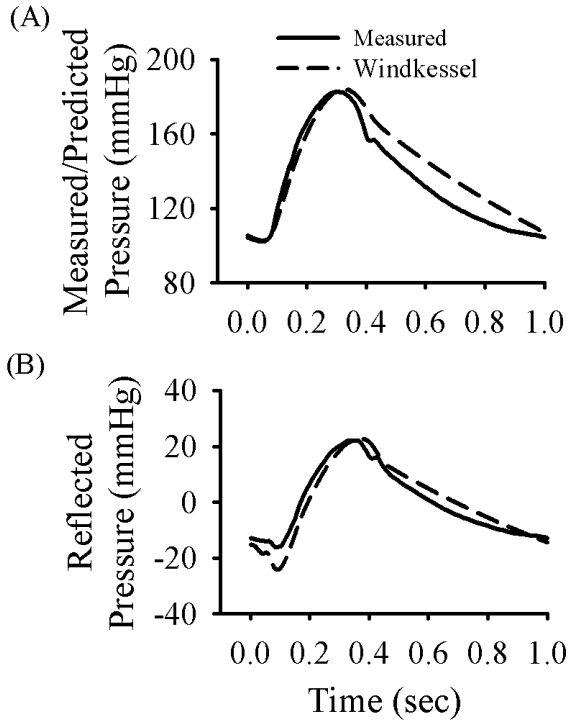

Figure A-11: Illustrative example used to show that the reflected pulse wave in severely hypertensive subjects results from degeneration into a classical Windkessel. (A) Pressure of a severely hypertensive 61 year old subject originally reported elsewhere (71) and the pressure estimated for its classical Windkessel equivalent (see Fig. A-7). (B) Reflected wave calculated from the more appropriate procedure (*Eq. 4.3*) for wave separation analysis and from the Windkessel equivalent. Similarity of the timing and morphology of the composite pressure reflected pulses indicates degeneration of systemic arterial system into a classical Windkessel.

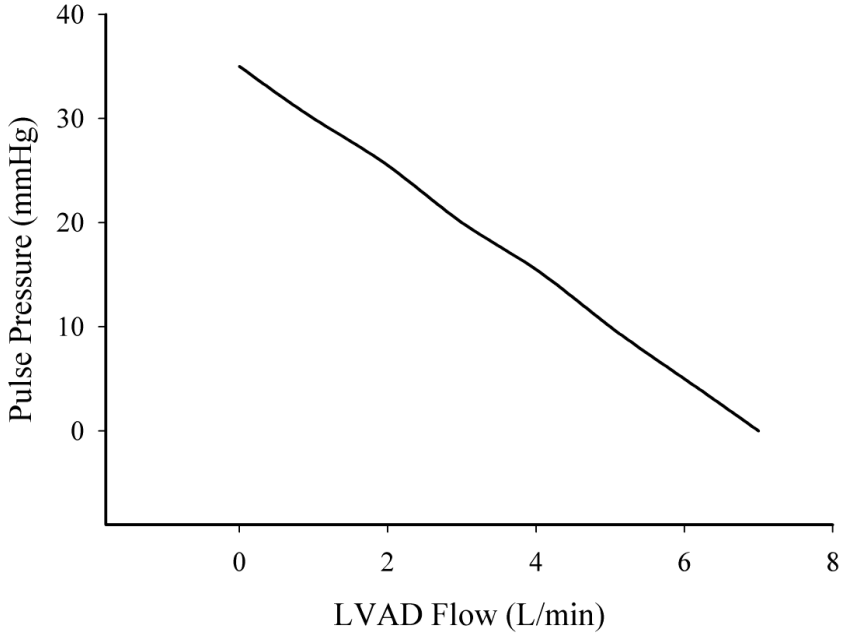

Figure A-12: Increases in LVAD flow decreases aortic pulse pressure in the realistic large-scale cardiovascular system model. At a critical value of LVAD flow, the aortic valve ceases to open, and aortic pressure loses pulsatility.

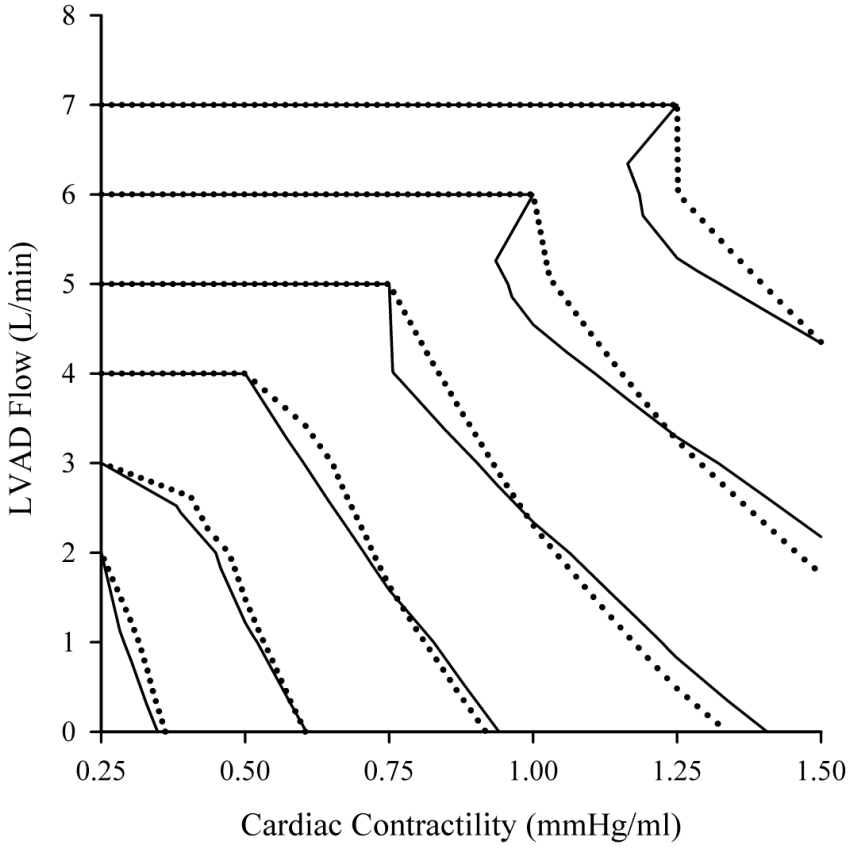

Figure A-13: Comparison of total aortic flow predicted by the realistic, large-scale arterial system model (─) with the approximate solution given by *Eq. 5.10*. (●) at different contractile states of the left ventricle (characterized by E_{max}) under various levels of LVAD flow. As ventricular contractility or LVAD flow increases, total aortic flow increases. Plateau in upper left quadrant indicates that ventricular contractility is too low to force open the aortic valve, and aortic flow is thus equal to LVAD flow.

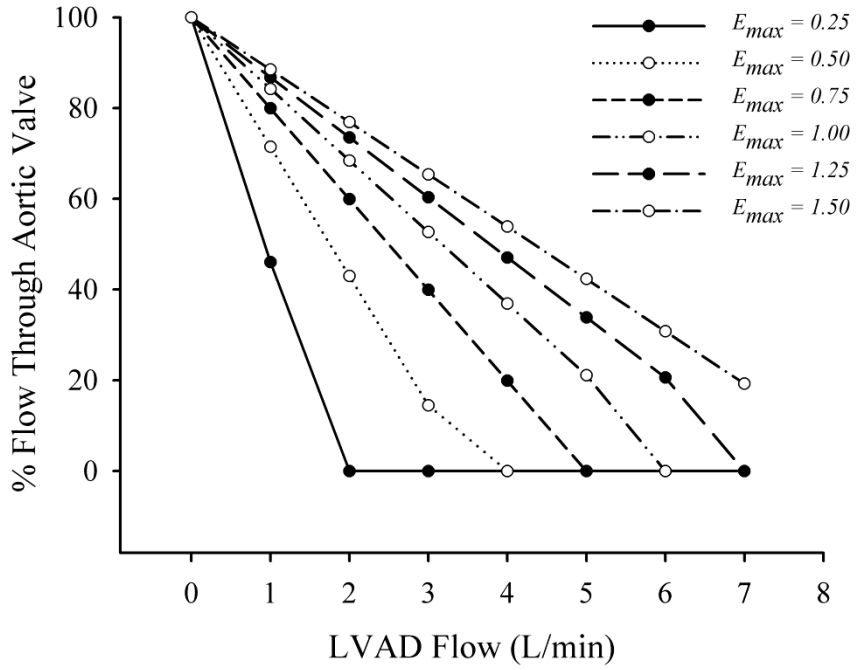

Figure A-14: Increasing LVAD flow decreases the percentage of total aortic flow that passes through the aortic valves [predicted from *Eq. 5.8*]. When LVAD flow (i.e., Q_{LVAD}) is high or when ventricular contractility (i.e., E_{max}) is low, aortic flow is entirely provided by the LVAD.

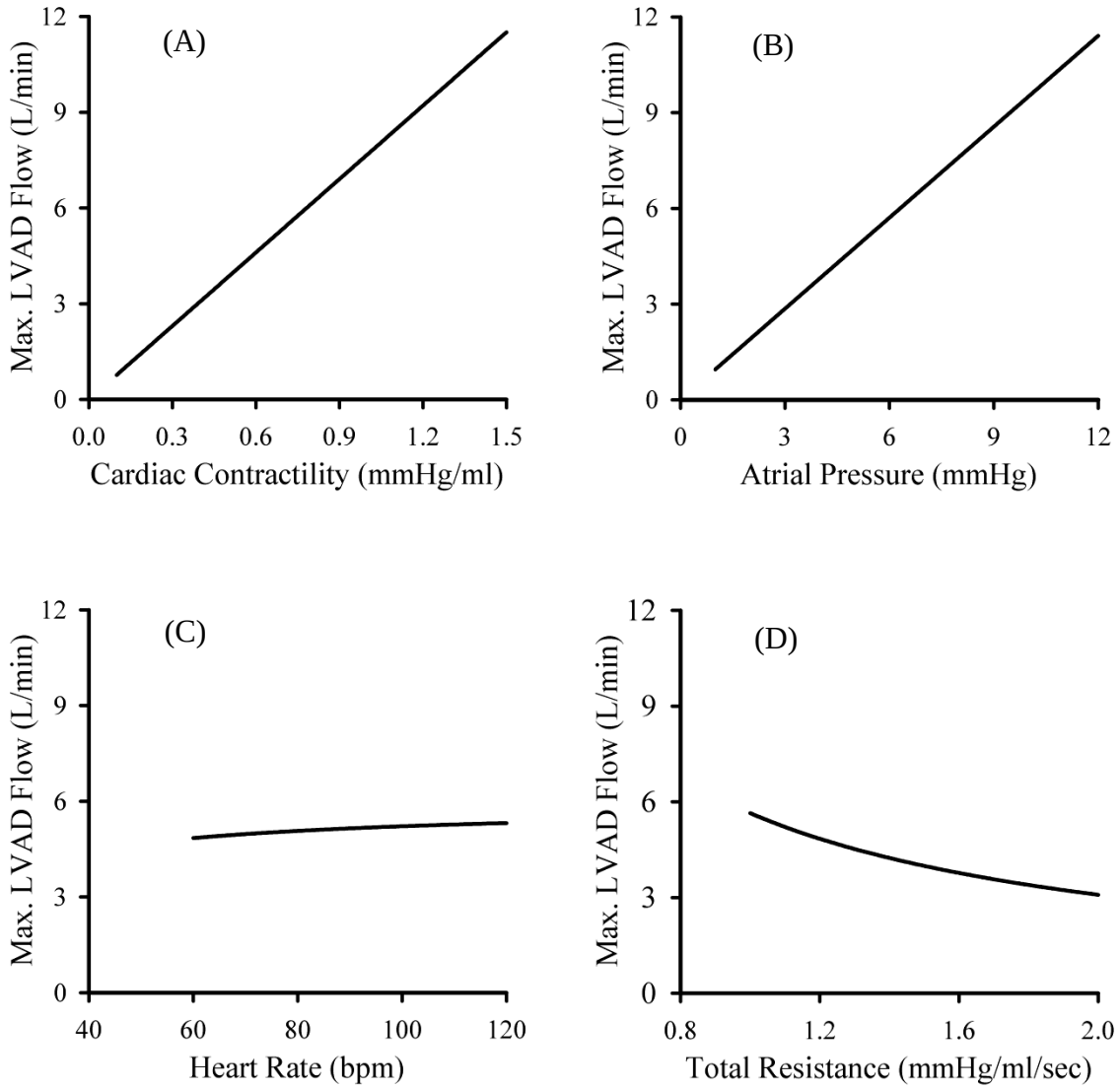

Figure A15: Illustration of how critical cardiovascular system parameters impact the maximum LVAD flow that ensures that the aortic valve opens during some portion of the cardiac cycle. This maximum LVAD flow [i.e., $Q_{LVADmax}$, *Eq. 5.11*] can be increased with (A) ventricular contractility (E_{max}), (B) atrial pressure (P_{atria}), (C) heart rate (HR), and decreased with (D) total systemic arterial resistance (R_{tot}).

VITA

Name:	Mohammad Waqar Mohiuddin
Address:	M.S. 4466, Physiology & Pharm., TAMU, College Station, TX 77843-4466.
Email Address:	physioneer@gmail.com
Education:	B.Sc., Mechanical Engineering, Bangladesh University of Engineering & Technology, 1998. M.S., Mechanical Engineering, Texas A&M University, 2002. Ph.D., Biomedical Sciences, Texas A&M University, 2008.
Expertise:	Pulsatile Hemodynamics, Human Physiology, Computer Aided Engineering, Finite Element Analysis, Mechanical Device Design.